Heterodyne performance and characteristics of terahertz MgB2hot electron bolometers

Journal of Applied Physics

Heterodyne performance and characteristics of terahertz MgB_2 hot electron bolometers

Cite as: J. Appl. Phys. **133**, 074503 (2023); https://doi.org/10.1063/5.0128791
Submitted: 30 September 2022 • Accepted: 30 January 2023 • Published Online: 17 February 2023

Y. Gan, B. Mirzaei, J. R. G. Silva, et al.

AIP Publishing

Journal of Applied Physics ARTICLE scitation.org/journal/jap

Heterodyne performance and characteristics of terahertz MgB_2 hot electron bolometers

Cite as: J. Appl. Phys. **133**, 074503 (2023); doi: 10.1063/5.0128791
Submitted: 30 September 2022 · Accepted: 30 January 2023 ·
Published Online: 17 February 2023

Y. Gan,[1,2,3] B. Mirzaei,[1,2,4] J. R. G. Silva,[1,2,3] S. Cherednichenko,[5] F. van der Tak,[1,2,3] and J. R. Gao[1,2,4,a)]

AFFILIATIONS

[1]SRON Netherlands Institute for Space Research, Niels Bohrweg 4, 2333 CA Leiden, The Netherlands
[2]SRON Netherlands Institute for Space Research, Landleven 12, 9747 AD Groningen, The Netherlands
[3]Kapteyn Astronomical Institute, University of Groningen, Landleven 12, 9747 AD Groningen, The Netherlands
[4]Optics Group, Department of Imaging Physics, Delft University of Technology, 2628 CJ Delft, The Netherlands
[5]Terahertz and Millimetre Wave Laboratory, Department of Microtechnology and Nanoscience, Chalmers University of Technology, SE-412 96 Gothenburg, Sweden

Note: This paper is part of the Special Collection Recognizing Women in Applied Physics.
a)Author to whom correspondence should be addressed: J.R.Gao@sron.nl

ABSTRACT

We have studied THz heterodyne detection in sub-micrometer MgB_2 hot electron bolometer (HEB) mixers based on superconducting MgB_2 films of ∼5 nm (HEB-A), corresponding to a critical temperature (T_c) of 33.9 K, and ∼7 nm (HEB-B), corresponding to a T_c of 38.4 K. We have measured a double sideband (DSB) receiver noise temperature of 2590 K for HEB-A and 2160 K for HEB-B at 1.6 THz and 5 K. By correcting for optical losses, both HEBs show receiver noise temperatures of ∼1600 K referenced to the front of anti-reflection (AR)-coated Si lenses. An intermediate frequency (IF) noise bandwidth of 11 GHz has been measured for both devices. The required local oscillator (LO) power is about 13 μW for both HEBs. We have also measured a DSB receiver noise temperature of 3290 K at 2.5 THz and 5 K but with an AR-coated lens optimized for 1.6 THz. Besides, we have observed a step-like structure in current voltage (IV) curves, which becomes weaker when the LO power increases and observable only in their differential resistance. Such a correlated structure appears also in the receiver output power as a function of voltage, which is likely due to electronic inhomogeneities intrinsic to the variations in the thickness of the MgB_2 films. Different behavior in the IV curves around the low bias voltages, pumped with the same LO power at 1.6 and 5.3 THz, was observed for HEB-B, suggesting the presence of a high-energy σ-gap in the MgB_2 film.

I. INTRODUCTION

Superconducting hot electron bolometer (HEB) mixers,[1] which consist essentially of a thin superconducting bridge embedded within a planar antenna on a chip, are currently the most sensitive heterodyne detectors for high-resolution spectroscopy at frequencies between 1 and 6 THz.[2] HEB mixers play a crucial role in astrophysics in this frequency region, which is rich in atomic, ionic, and molecular spectral lines that, for example, probe the origin of galaxies, stars, and planets.[3] Among them, the fine structure line of [OI] at 4.7448 THz probes the star formation process, which is the most important cooling line in the interstellar medium (ISM) for gas clouds with densities of $n > 10^4$ cm^3 and the temperature of > 200 K. Detection of spectrally resolved [OI] lines requires a heterodyne receiver with high sensitivity, namely, a low receiver noise temperature, and also a large intermediate frequency (IF) bandwidth of the mixer, which should, for example, be as large as 6 GHz if the observations target the center of the Milky way.

HEBs based on superconducting NbN thin films with a critical temperature (T_c) of 9–10 K have been so far the only mixing detectors at 1–6 THz and have been successfully applied in the airborne telescope of Stratospheric Observatory for Infrared Astronomy (SOFIA),[4] the balloon-borne telescope of Stratospheric Terahertz Observatory 2 (STO-2),[5] and the Herschel Space Observatory.[6] They will be flown in the upcoming NASA balloon-borne THz observatories, GUSTO[7] and ASTHROS,[8] and are planned for the recently proposed NASA far-IR space mission of OASIS,[9] which

will have an unprecedented large telescope of 14-m diameter, and also for the mission concept of a far infrared spectroscopy surveyor (FIRSS).[10]

NbN HEB mixers have demonstrated high sensitivities with double sideband (DSB) receiver noise temperatures (T_{rec}^{DSB}) approaching a few times the quantum noise.[11] The high sensitivity is essential since the integration time of an observation is proportional to the square of T_{rec}^{DSB}. The NbN HEB mixers offer an IF bandwidth typically not more than 4 GHz, which is limited by the thermal time determined by the electron–phonon scattering time[12] (14 ps at a T_c of 9.5 K) and the phonon escape time from the film to the substrate. Such a bandwidth can meet many scientific goals but is insufficient for detecting emission lines at the high end of the 1–6 THz region, such as the [OI] lines emitted from the center of the Milky Way or most emission lines from external galaxies.[3] Furthermore, a large IF bandwidth is preferred since it can cover more spectral lines within one single measurement, which makes the observations more efficient and calibration more accurate. NbN HEBs require a low operating temperature of about 4 K, which can be provided either using a liquid helium vessel or a mechanical pulse tube, both of which increase considerably the cost and complexity of a space mission. Both factors can be reduced significantly by raising the operating temperature to, for example, 20 K, which is reachable by the compact, low mass, low dissipation, and space-qualified Stirling cooler.[13] This will increase the design freedom, ambitions, and scientific return for new space instruments, for example, an interferometer with a number of telescopes in space[14] or new observatories from space for Earth atmosphere.[15]

Schottky diode mixers operated at room temperature work also at the THz region. Unfortunately, they usually have higher noise levels than superconducting mixers. In particular, it seems to be difficult to realize sensitive Schottky mixers at the high end of the 1–6 THz range.[16] HEB mixers based on high T_c Yttrium-barium-copper-oxide (YBCO) thin film superconductors may offer an elevated operating temperature such as the liquid-nitrogen temperature, but they have so far not demonstrated reliable, low noise performance at THz frequencies due to chemical non-stability and aging effects in the thin YBCO films.[17]

With a T_c of about 40 K and a short electron–phonon interaction time (1–2 ps),[18] superconducting magnesium diboride (MgB_2)[19] opens a new avenue for HEB mixers with enlarged IF bandwidths and high operating temperatures of 20 K or above. On the other hand, because of the double superconducting gaps in MgB_2,[20] the HEB structure can explore the electrodynamic process by applying THz radiation across the two bands, which may offer unique opportunities to optimize the HEB operating frequency.

Thin MgB_2 films with a T_c even higher than the value of the bulk[19] can be grown using different techniques, out of which hybrid physical chemical vapor deposition (HPCVD) has shown the highest T_c for ultra-thin films, i.e., <20 nm.[21] MgB_2 films have a hexagonal structure with a lattice constant in the *ab* plane, matching closely to 6H-SiC substrates, facilitating epitaxial growth of *c*-axis-oriented MgB_2 films with the *ab* plane in parallel with the substrate. Like in bulk, MgB_2 films show two superconducting gaps,[20] namely, the low-energy π-band, Δ_π, and the high energy σ-band, Δ_σ, which govern two parallel conductivities along the film. Uniquely, despite the two distinct gaps of different magnitudes, there is only one single T_c of the material, caused by finite coupling between the two gaps.[19]

An HPCVD-grown clean MgB_2 film with a low impurity level has shown double gaps[20] in the far-IR optical response covering the range of its superconducting gap frequencies in the 0.7–4 THz range for the *ab* plane of MgB_2. However, it is known to be difficult to find the signature of the double gaps in the far-IR response measurements if the films have impurities, defects, or dirty spots (called the dirty film here), resulting in intra-band as well as inter-band scattering. Because of scattering, dirty MgB_2 films in Refs. 20 and 22 fail to show double gaps in a far-IR response measurement, but only one gap, which is dominated by the low-energy π-band. An MgB_2 film (34 K) in Ref. 22 shows one gap of 2.5 meV that is close to Δ_π. Why there are more impurity scatterings in some films is not fully clear yet. The strong impurity scattering might be due to exposure of the films to moisture in the air, which causes degradation that could happen easily and quickly, e.g., within a few minutes.[23]

Toward MgB_2 HEB mixers, ultrathin films with a high T_c have been developed. The reduced thickness is essential to decrease the phonon escape time to the substrate. All existing MgB_2 HEB mixers have a similar layout, namely, MgB_2 patterned as a sub-μm sized or μm-sized bridge, which is electrically connected to a broad band Au spiral antenna patterned on a dielectric, semi-insulating silicon carbide (SiC) substrate. The optical loss for a SiC substrate has been evaluated experimentally up to 6 THz and is considered generally low.[24,25] For example, it was reported that the optical loss at room temperature is negligibly low up to 2.5 THz but starts to increase afterward.[24] However, no such data are yet available at cryogenic temperatures, where, in general, the optical loss is expected to be reduced.

Table I summarizes all the MgB_2 HEBs reported so far in the literature, with their T_{rec}^{DSB} either with or without correcting for optical losses and IF bandwidths. They are highlighted as follows: Cherednichenko *et al.* reported the first MgB_2 HEB in 2007, which was fabricated using a 20 nm molecular beam epitaxy (MBE) grown film with a T_c of 22 K, resulting in a measured T_{rec}^{DSB} of 11 000 K at 1.6 THz and a mixer gain bandwidth (GBW) of 2.3 GHz.[26] Cunnane *et al.* reported MgB_2 HEB mixers based on 10–20 nm HPVCD grown films with a T_c of 33–38 K, which give a measured T_{rec}^{DSB} of 3900 K at 600 GHz and a GBW of 6.9 GHz.[29] An HEB mixer based on a MgB_2 film of 7 nm with a T_c of 34 K, thinned from a thicker film by Ar ion milling, gave a T_{rec}^{DSB} of 3600 K at 1.9 THz and an IF noise bandwidth (NBW) of 6.5 GHz.[31] A T_{rec}^{DSB} of 930 K at 1.6 THz [after correcting optical losses before the Si lens and also assuming its anti-reflection (AR) coated] together with a high NBW of 11 GHz in an MgB_2 HEB mixer was reported at 5 K in Ref. 32, which was based on an 6 nm thick, HPCVD grown film with a T_c of 31 K. Very recently, we have reported a measured T_{rec}^{DSB} of 3960 K at 5.3 THz (the highest frequency so far) with 20 K operating temperature using an ∼7 nm HPVCD grown film with a T_c of 38.4 K. This T_{rec}^{DSB} gives a DSB mixer noise temperature (T_{mix}^{DSB}) of 1470 K, derived from a standard relation between the two performance parameters by subtracting the noise and loss contribution from all the optics and the noise from the IF chain using the measured receiver gain.[34]

The improvement in the IF bandwidth of MgB_2 HEBs is striking. For example, 11 GHz in Ref. 32 and 13 GHz in Ref. 33 noise

TABLE I. Summary of all the MgB_2 HEBs reported in the literature. The table includes the frequency of a local oscillator (LO) f_{LO}, the measured receiver noise temperature T_{rec}^{DSB}, the IF bandwidth IFB (either measured GBW or NBW is indicated inside the bracket in the table), the operating temperature T_{bath}, the critical temperature of the MgB_2, the film thickness t, the MgB_2 growth method, and the reference. The superscript "corr" associated to the T_{rec}^{DSB} means that the value is not the directly measured value of T_{rec}^{DSB} but the one after correcting or removing some losses in the optical path.

f_{LO} (THz)	T_{rec}^{DSB} (K)	*IFB* (GHz)	T_{bath} (K)	T_c (K)	t (nm)	Grown method	Ref., year
1.6	11 000	2.3 (GBW)	4.2	22	20	MBE	Ref. 26, 2007
0.6	$700^{corr.}$	2.2–3 (NBW)	4.2	8.5	10	MBE	Ref. 27, 2015
1.6	$1700^{corr.}$ $2150^{corr.}$	5 (NBW)	4.2 12	22.5	20	MBE	Ref. 28, 2016
0.6	3900	6.9 (GBW)	9	33–38	10–20	HPCVD	Ref. 29, 2015
0.69	$4300^{corr.}$	6 (GBW)	23	35	15	HPCVD	Ref. 30, 2016
0.6 1.9	2000 3600	6.5 (NBW)	8.2	34	7	HPCVD	Ref. 31, 2017
1.6	$930^{corr.}$ $1120^{corr.}$ $1630^{corr.}$	11 (NBW)	5 15 20	31	6	HPCVD	Ref. 32, 2017
1.6	$1000^{corr.}$	13 (NBW)	5	34	5	HPCVD	Ref. 33, 2019
5.3	3960 $2720^{corr.}$ $2400^{corr.}$	10 (NBW)	20 20 6	38.4	7	HPCVD	Ref. 34, 2021
3.3	$2600^{corr.}$ $5000^{corr.}$	…	5 25	34–36	10	HPCVD	Ref. 35, 2022

bandwidth at 1.6 THz. An IF gain bandwidth of 13–14 GHz measured at an elevated temperature using a cryo-probe station[33] and with a 90-GHz local oscillator (LO) together with the spectrum of the output noise, suggesting a possible noise bandwidth exceeding 20 GHz for a proper IF-matched HEB-low noise amplifier (LNA) combination. Therefore, current MgB_2 HEBs offer 3–4 times larger noise bandwidth than NbN HEBs. Low noise performances have been also demonstrated in MgB_2 HEBs and are extremely encouraging. However, the obtained T_{rec}^{DSB} from MgB_2 HEBs are still higher than what is reported from NbN HEBs mixers. For example, at 1.6 THz, the best noise temperature from MgB_2 (Ref. 32) is a factor of 1.8 higher than a NbN HEB mixer,[36] while at 5.3 THz, this factor is about 2.5 if MgB_2 is operated at 20 K and becomes a factor of 2.1 when it is operated at 6 K or below.[34] To further improve T_{rec}^{DSB}, one needs to explore the device physics, in particular, electrodynamical processes at THz unique to MgB_2 nature such as the high and the double gap feature.

In this work, we will focus on experimental determination of the heterodyne performance and device characteristics of MgB_2 HEB mixers at 1.6 THz. The heterodyne performance, including the receiver noise temperature and IF bandwidth, was characterized at 5 or 6 K. The HEBs are fabricated on two ultrathin HPCVD films and with two slightly different fabrication processes. We also present experimental data on current–voltage (IV) under different pumping levels and also discuss the origin of the observed structures in the IV curves. Finally, we address the double-gap effect in MgB_2 HEBs by using higher frequency LOs at 5.3 THz in comparison to the data at 1.6 THz.

II. HEB DEVICES AND FABRICATION

A. HEB-A

The MgB_2 film used in our study is developed at Chalmers University of Technology using a HPCVD method. The detailed deposition process can be found in Ref. 37. The nominal thickness of the MgB_2 film is ~5 nm according to the deposition rate and time. By lack of direct measurements, this number, including the thickness of the second film used in this paper, is merely indicative of a proportionally longer deposition time. The substrate is a 320 μm thick 6H-SiC (0001), which gives only a 0.42% lattice mismatch to the MgB_2 film.[38] To minimize oxidation, when taken out from the HPCVD chamber, the film was immediately loaded into a sputter machine, where it was coated with an Au layer (20 nm) after a short, *in situ* sputter cleaning of its surface. HEB fabrication takes place at Delft University of Technology and starts with the definition of the contact-pads with e-beam lithography (EBL) and Au evaporation in combination with a lift-off process. Then, the spiral antennas are defined using a similar process but by evaporating a thicker Au layer followed by a layer of Ti on top. The latter is to prevent etching of the Au antenna during Ar Ion beam milling etching (IBME) to define the MgB_2 bridge width. The Au protecting layer is then physically removed using IBME, followed by sputtering a 40 nm Si_3N_4 layer, which intends to prevent oxidation of MgB_2 in the following fabrication steps. The resist mask for the definition of the sub-micrometer bridge is then patterned using EBL. Finally, uncovered Si_3N_4 and MgB_2 are etched away using ion-milling, where a sub-μm MgB_2 bridge between the two contact pads is formed and the device fabrication is, thus, completed.

Figure 1(a) shows a top view of a completed MgB_2 HEB imaged by a scanning electron microscope (SEM), together with a 3D drawing focused only on the MgB_2 bridge and contact pads. For HEB-A (numbered as MgB2_BM1_1C), the MgB_2 bridge has a width of 0.4 μm and a length of 1.2 μm. The widths and lengths of HEB-A together with HEB-B are summarized in Table II. The narrow bridge is to minimize the HEB volume and, hence, to reduce the required LO power. It has a room temperature resistance (R_{RT}) of 84 Ω and a low temperature normal-state resistance (R_N) of 62 Ω, taken above T_c. The residual resistance ratio ($RRR = R_{RT}/R_{40\,K}$) of the HEB is found to be 1.35. The MgB_2 HEB has a T_c of 33.9 K, and a critical current of 0.9 mA at 5 K, giving a critical current density of 4.5×10^7 A/cm^2.

We found an increase in the R_{RT} of HEB-A from 84 to 108 Ω after it was exposed to normal air and a wet environment. The R_N and the critical current are also changed and become 78 Ω and 0.68 mA, respectively. Since MgB_2 is known to be sensitive to water, our Si_3N_4 layer in terms of thickness and width is not sufficient to protect the MgB_2.

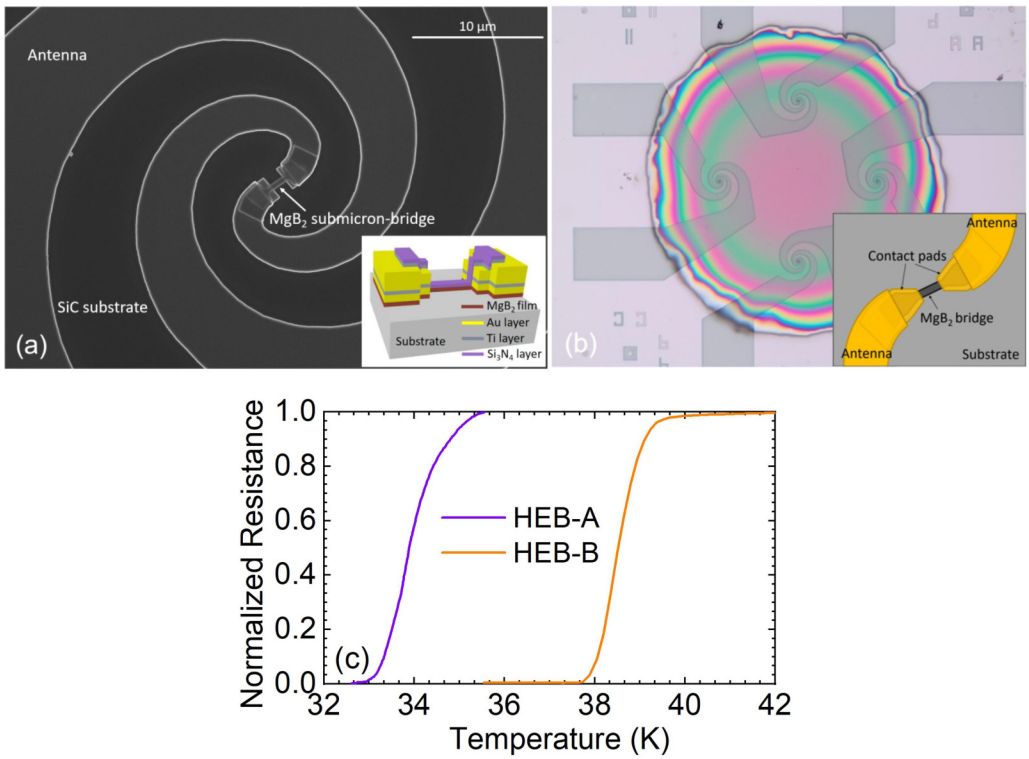

FIG. 1. (a) SEM micrograph of a spiral antenna coupled MgB_2 HEB from the same batch as HEB-A. The inset is a 3D model of the MgB_2 submicrometer-bridge and part of the contact pads and the spiral antenna. The colors indicate different materials. (b) Optical micrograph of a device chip, containing four HEBs, from the same batch as HEB-B. A layer of 500 nm thick Si_3N_4 is sputtered to cover the surface of the chips except for the bonding pads to isolate MgB_2 bridges from water and air. The inset in (b) is an artistic impression of HEB-B, which shows exactly the same layout as the design. (c) The resistances of HEB-A and HEB-B as a function of temperature, where the critical temperatures are 33.9 and 38.4 K, respectively.

B. HEB-B

To eliminate the device degradation due to the exposure to air, we fabricated another batch of HEB devices with a ∼7 nm thick MgB_2 film grown by HPCVD. We applied a very similar fabrication process as for HEB-A except for a few differences. The Au layer of 20 nm is removed using IBME, followed immediately by depositing a layer of 80 nm thick Si_3N_4 to avoid the oxidation of MgB_2. Before dicing the HEB wafer, a 500 nm thick Si_3N_4 is sputtered to cover the surface of the chips except for the bonding pads to isolate MgB_2 bridges from water and air. Each chip contains four MgB_2 HEBs as shown in Fig. 1(b), where the inset shows an HEB of 285 nm width and 850 nm length on a 320 μm thick SiC substrate. The tapered contact-pads are designed to reduce the reactance.[39] HEB-B (MgB2_BM3_2b) has a R_{RT} of 92 Ω, while R_N equals 51 Ω. The T_c is 38.4 K and the RRR value is 1.8. The critical current of the HEB is 1.3 mA at 5 K, corresponding to a current density of 6.5×10^7 A/cm^2, which is a factor of 1.4 higher than HEB-A and a factor of 3 higher than what was reported in Ref. 32.

The same antenna design was used in both batches to match ideally an HEB impedance of 80 Ω, with an upper cut-off frequency of ≥6 THz.[40]

TABLE II. Width, length, and low temperature normal state resistance R_N of two HEB devices from two batches. They are based on two MgB_2 films with different thicknesses and T_c: ∼5 nm and 33.9 K for HEB-A and ∼7 nm and 38.4 K for HEB-B.

Devices	HEB-A (MgB2_BM1_1C)	HEB-B (MgB2_BM3_2b)
Width (μm)	0.4	0.285
Length (μm)	1.2	0.85
R_N (Ω)	78	51

III. MEASUREMENT SETUPS

A. Setup-A in air for receiver noise temperatures

Figure 2 shows a schematic of setup-A, the experimental setup in air for measuring the T_{rec}^{DSB} of MgB_2 HEB-A. The method is based on the Y-factor technique[40] using THz calibration sources of hot (@293 K) and cold (77 K) blackbody loads. A far-infrared (FIR) gas laser, optically pumped by a CO_2 laser, acts as a LO, which can emit lines at different frequencies by combining a specific gas with a CO_2

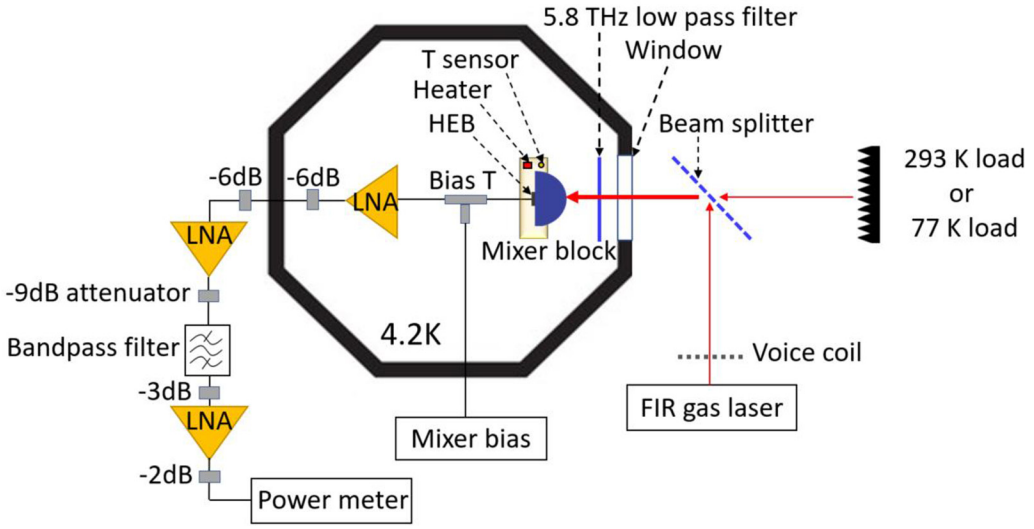

FIG. 2. Schematics of setup-A that is the measurement setup in air for measuring T_{rec}^{DSB} of the HEB-A mixer. It is measured at f_{if} = 2 GHz with a narrow band (Δf_{if}) of 100 MHz, defined by the bandpass filter.

pumping line. We used the line at 1.6 (1.626) THz with CH_2F_2 gas and the line at 2.5 (2.523) THz with CH_3OH gas.

A voice coil attenuator located in front of the gas laser is used to vary the LO power absorbed by the HEB.[41] The T_{rec}^{DSB} of HEB-A was measured at 1.6 and 2.5 THz. The signal and the LO are combined by a 6 μm thick Mylar beam splitter, passing through an ultra-high-molecular-weight polyethylene (UHMW-PE) window at 300 K and a QMC multimesh low pass filter with a cut-off frequency of 5.8 THz at 4 K, then reaching the Si lens-coupled HEB. The HEB chip is glued to the back side of an elliptical Si lens[42] with an AR coating. The coating is a 28 μm thick Parylene-C, which is designed for 1.6 THz. The lens-antenna HEB mixer is mounted on a metal block, which is anchored on the 4 K plate of a liquid helium cryostat. Their interface is on purpose made thermally resistive so that the operating temperature can be raised locally. A heater together with a temperature sensor is installed on the mixer block to elevate the local temperature of the mixer from the bath temperature up to T_c. The optical losses contained in the optical path at two frequencies, 1.6 and 2.5 THz, are presented in Table III, where the optical loss of the AR-coated Si lens is simulated using COMSOL Multiphysics, taking the absorption coefficients of Parylene C of 10.5 cm^{-1} at 1.6 THz and 16.2 cm^{-1} at 2.5 THz into consideration.[43,44]

A 0.2–18 GHz cryogenic Bias-Tee is used to give DC bias to the HEB and transmit the intermediate frequency (IF) to an amplifier chain. The latter includes a 0.1–14 GHz cryogenic LNA (LNA#1, at 4.2 K) with a 39 dB gain, a 0.1–14 GHz room temperature (RT) LNA (LNA#2) with a gain of 42 dB, and a 0.1–12 GHz RT LNA (LNA#3) with a gain of 30 dB. A bandpass filter (BPF) with 100 MHz bandwidth is used to filter the IF signal at 2 GHz. Between each two elements, there is an attenuator to suppress standing waves. The total gain of the IF chain is 85 dB (at 2 GHz), and the noise temperature contribution from the IF chain to the mixer is 4.5 K at 2 GHz. The amplified IF signal is read out by a power meter.

B. Setup-B in vacuum, with a circulator for receiver noise temperatures

Figure 3 shows a schematic of our measurement setup-B in vacuum for characterizing T_{rec}^{DSB} and receiver conversion gain G_{rec}^{DSB} at 1.7 GHz for the HEB-B device, which is reproduced from Gan *et al.*, Appl. Phys. Lett. **119**, 202601 (2021). Copyright 2021 AIP

TABLE III. Signal losses in the components of the optical path (from the hot/cold loads to the HEB-A chip), including the 30 cm air path (L_{air}), the 6 μm Mylar beam splitter (L_{BS}) at 300 K, the window (L_{window}) at 300 K, the 5.8 THz low pass filter (L_{filter}) at 4 K, the AR-coated Si lens (L_{lens}) optimized for 1.6 THz at 4 K, and the coupling between antenna and HEB when we assume the normal resistance of the HEB as the RF impedance. Components in orange fields are at room temperature, and components in blue fields are at 4 K. The measured T_{rec}^{DSB} together with the corrected receiver noise temperature $T_{rec}^{corr.}$ referenced to the front of AR-coated Si lenses at two frequencies, to be described in Sec. IV, are also presented.

LO frequency (THz)	L_{air} (dB)	L_{BS} (dB)	L_{window} (dB)	L_{filter} (dB)	L_{lens} (dB)	$L_{coupling}$ (dB)	T_{rec}^{DSB}(K)	$T_{rec}^{corr.}$(K)
1.6	0.65	0.27	0.37	1.00	0.35	0.02	2590	1596
2.5	0.38	0.56	0.63	0.33	1.11	0.11	3290	1866

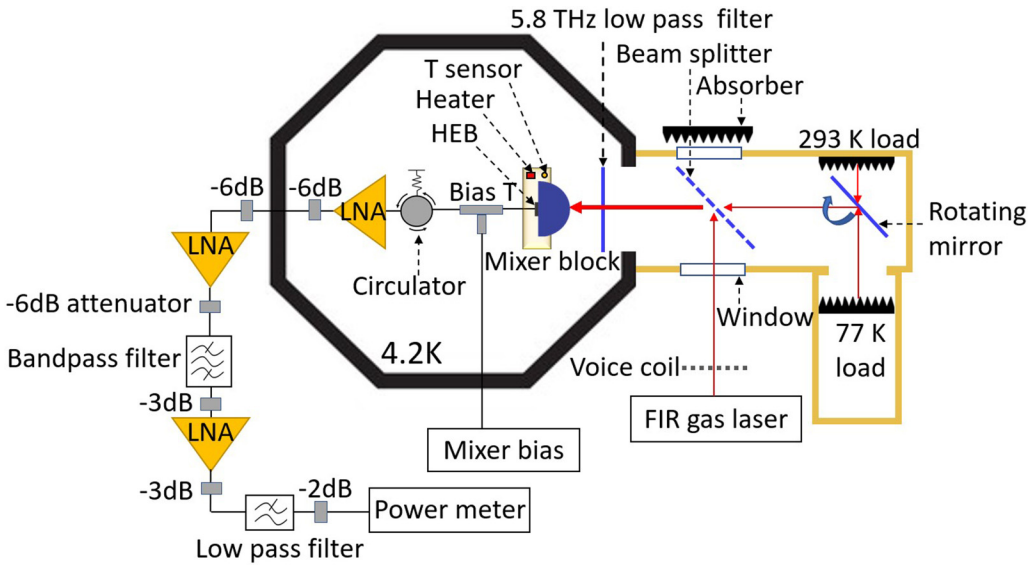

FIG. 3. Schematics of setup-B that is the setup in vacuum for measuring the T_{rec}^{DSB} and G_{rec}^{DSB} of the HEB-B device at f_{if} = 1.7 GHz (Δf_{if} = 85 MHz). There is a circulator in the IF chain, which is dedicated to G_{rec}^{DSB} measurements. The hot/cold loads and the Mylar beam splitter are placed in a vacuum enclosure, attached to the cryostat. A rotating mirror is used to switch between the hot and cold loads. Reproduced from Gan *et al.*, Appl. Phys. Lett. **119**, 202601 (2021). Copyright 2021 AIP Publishing LLC.

Publishing LLC. This setup is in principle the same as setup-A, except for that the hot/cold loads and the Mylar beam splitter are placed in a vacuum enclosure, attached directly to the cryostat where no cryostat window is needed. The optical losses contained in the optical path at 1.6 THz, are presented in Table IV. The vacuum setup is applied for the 1.6 THz measurement although originally it was to avoid the air absorption loss (~1 dB) at 5.3 (5.246) THz with CH_3OH gas.[34]

The IF chain is similar to setup-A. However, we introduce a circulator with a bandwidth from 1.3 to 1.7 GHz between the bias-tee and LNA#1. The circulator is necessary for an accurate measurement of the HEB receiver gain G_{rec}^{DSB} since it prevents standing waves between the HEB and the LNA. Since we measure the T_{rec}^{DSB} of the device at 1.7 GHz, we use a bandpass filter (operated at 1.7 GHz in this case) in the room temperature part of the IF chain. But the bandpass filter is not capable of blocking the signals beyond 5 GHz, which adds noise to the measurements at 1.7 GHz; thus, we add a low pass filter with a cut-off frequency of 2.2 GHz after the bandpass filter.

The IF chain has a total gain of 85 dB and a noise temperature of 4.7 K at 1.7 GHz. We performed the measurements of T_{rec}^{DSB} and G_{rec}^{DSB} at 1.7 GHz instead of 2 GHz for HEB-A (in setup-A) because we have only the circulator up to 1.7 GHz available.

C. Setup-C for determination of the IF bandwidth

To measure T_{rec}^{DSB} over a wider range of IF frequencies to obtain an IF bandwidth of the HEB, the bandpass filter and RT LNA#2 are removed from setup-A, while the circulator, RT LNA#2, bandpass filter, and a low pass filter, are removed from setup-B. Furthermore, the power meter is replaced by a spectrum analyzer, which records the receiver output power vs IF in response to either the hot load or cold load from 0.1 to 14 GHz at high spectral resolution. Then, the receiver noise temperature vs IF can be obtained by applying the Y-factor method.

IV. MEASUREMENT RESULTS

A. Unpumped and pumped IVs

At an operating temperature of 5 K and with the LO at 1.6 THz, two sets of IV curves from zero LO power to fully pumped (driving the HEB to the normal state) for HEB-A and HEB-B are measured and shown in Fig. 4. Within the optimal operating region, which is 6–10 mV and 0.27–0.33 mA for HEB-A and 2–5.5 mV and 0.17–0.28 mA for HEB-B, the sensitivity of the HEB degrades by only 5% from its best value, which is determined

TABLE IV. Losses of the components in the optical path from the hot/cold loads to the HEB-B at 1.6 THz in the vacuum set, including the 6 μm Mylar beam splitter (BS) (L_{BS}) at 300 K, the 5.8 THz low pass filter (L_{filter}) at 4 K, the coated Si lens (L_{lens}) at 4 K, and the power coupling between antenna and HEB by assuming the HEB RF impedance to be the same as the R_N. Components in orange fields are at room temperature, and components in blue fields are at 4 K. The measured T_{rec}^{DSB}, the corrected receiver noise temperature $T_{rec}^{corr.}$ referenced to the front of AR coated Si lens, and the mixer noise temperature T_{mix}^{DSB} are also included (to be described in Sec. IV).

LO frequency	L_{BS} (dB)	L_{filter} (dB)	L_{lens} (dB)	$L_{coupling}$ (dB)	T_{rec}^{DSB}(K)	$T_{rec}^{corr.}$(K)	T_{mix}^{DSB}(K)
1.6 THz	0.27	1.00	0.35	0.35	2160	1634	1319

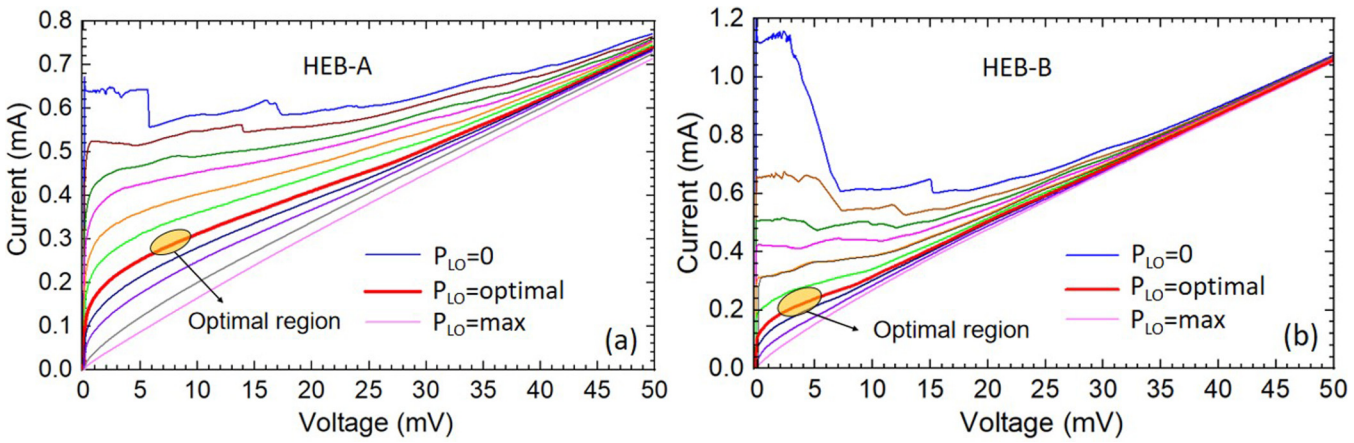

FIG. 4. IV curves of the MgB_2 HEB mixers at 1.6 THz with different applied LO powers at 5 K operating temperature. (a) IV curves of HEB-A. At the optimal operating point, the required LO power is 13.6 μW. (b) IV curves of HEB-B. At the optimal operating point, the required LO power is 12.5 μW. The yellow circle indicates the optimal operating region derived from Fig. 5. Both HEBs show step-like structures in their IV curves, which become weaker with increasing LO power.

by measuring the T_{rec}^{DSB} at different bias voltages. The optimal LO power $P_{LO,opt}$ (i.e., corresponding to the lowest T_{rec}^{DSB}) as absorbed by the HEB was determined by the standard isothermal technique:[45] 13.6 μW for HEB-A and 12.5 μW for HEB-B. A smaller bridge volume in HEB-B as compared to HEB-A compensates for its higher T_c, hence resulting in nearly the same $P_{LO,opt}$.

Reproducible step-like structures can be observed in underpumped IV curves of both HEBs below 20 mV in Fig. 4. The amplitudes of the current steps reduce with increasing LO power. Around optimal IV curves ("optimal region" in Fig. 4), no such features seem to be present. However, as it will be discussed in Sec. IV C, these structures persist and can be seen from the differential resistance (dV/dI) as well as in the $P_{hot} - V$ and $P_{cold} - V$ curves, where $P_{hot,cold}$ is the receiver output power when the HEB is irradiated by the hot load or the cold load.

B. Receiver noise temperature for a given bias voltage at 1.6 THz

To obtain a T_{rec}^{DSB} based on the Y-factor, P_{hot} or P_{cold} is measured at the same IV-point. For a fixed bias voltage (V), the dc current (I) through the HEB is defined by the LO power absorbed in the HEB. The accuracy of the P_{hot}/ P_{cold} measurements is dependent on the LO power stability, which is not a trivial task at THz frequencies. In order to mitigate this issue, we utilized a method introduced in Ref. 41. Instead of stabilizing the power of the FIR gas laser we intentionally sweep its power (using a voice-coil actuator), while simultaneously recording P_{hot} (or P_{cold}) and the bias current.[46] Using this method, the error of the T_{rec}^{DSB} measurement of a HEB is within 5%. To find the minimum T_{rec}^{DSB}, we conduct this exercise at a number of bias voltages. The results at the fixed bias voltage of 8 mV for HEB-A and 2.5 mV for HEB-B are shown in Figs. 5(a) and 5(b), where P_{hot} and P_{cold} are plotted as a function of the current together with their polynomial fitted curves. The latter are used to determine the T_{rec}^{DSB}, plotted in the same figures, from which we select the minimum T_{rec}^{DSB}. We have carried out such measurements at a number of bias voltages to obtain the minimum T_{rec}^{DSB} at each bias voltage, where the LO power varies. The results are summarized in Figs. 5(c) and 5(d). Because of variable LO power, here the dependence of T_{rec}^{DSB} on voltage is different from that in Fig. 6 to be presented in Sec. IV C. The lowest T_{rec}^{DSB} for HEB-A is 2590 K (at 2 GHz) when it is biased at 8 mV and 0.3 mA and the lowest T_{rec}^{DSB} for HEB-B is 2160 K (at 1.7 GHz) when it is biased at 2.5 mV and 0.22 mA. Both measured T_{rec}^{DSB} are listed in Tables III and IV.

Figures 5(e) and 5(f) show the minimum T_{rec}^{DSB} at different operating temperatures from 5 to 20 K. For HEB-A, when the operating temperature increases, the T_{rec}^{DSB} stays nearly the same from 5 to 10 K, but it increases by 15% at 15 K and 37% at 20 K. For HEB-B, the T_{rec}^{DSB} increases only by 17% when the operating temperature increases from 5 to 20 K. The slower increase in HEB-B should be related to the higher T_c of the HEB-B and has also been seen in the 5.3 THz measurements of the same device.[34] Previously, T_{rec}^{DSB} vs operating temperature T in MgB_2 HEB mixers was studied at 0.6–3.3 THz[31–33,35,47] where the possible effect of a high T_c on the T_{rec}^{DSB} vs T behavior was pointed out. Because T_c of HEB-B (38.4 K) used in our study is significantly higher, we now demonstrate that the heterodyne sensitivity of the MgB_2 HEB degrades only marginally for temperatures up to 20 K.

At the optimal operating point where the T_{rec}^{DSB} is the lowest, the $G_{rec}^{DSB}(= G_{opt}G_m^{DSB})$ for HEB-B is measured by using the U-factor,[48] which is the ratio between the receiver output power when the HEB is at its operating point and the receiver output power when it is in its superconducting state. The G_m^{DSB} is found to be −7.8 dB by subtracting all the optical losses from the derived G_{rec}^{DSB}. However, we could not get a reliable G_m^{DSB} for HEB-A (using setup-A) because of the standing waves between the HEB and LNA. Therefore, no G_m^{DSB} data for HEB-A are present.

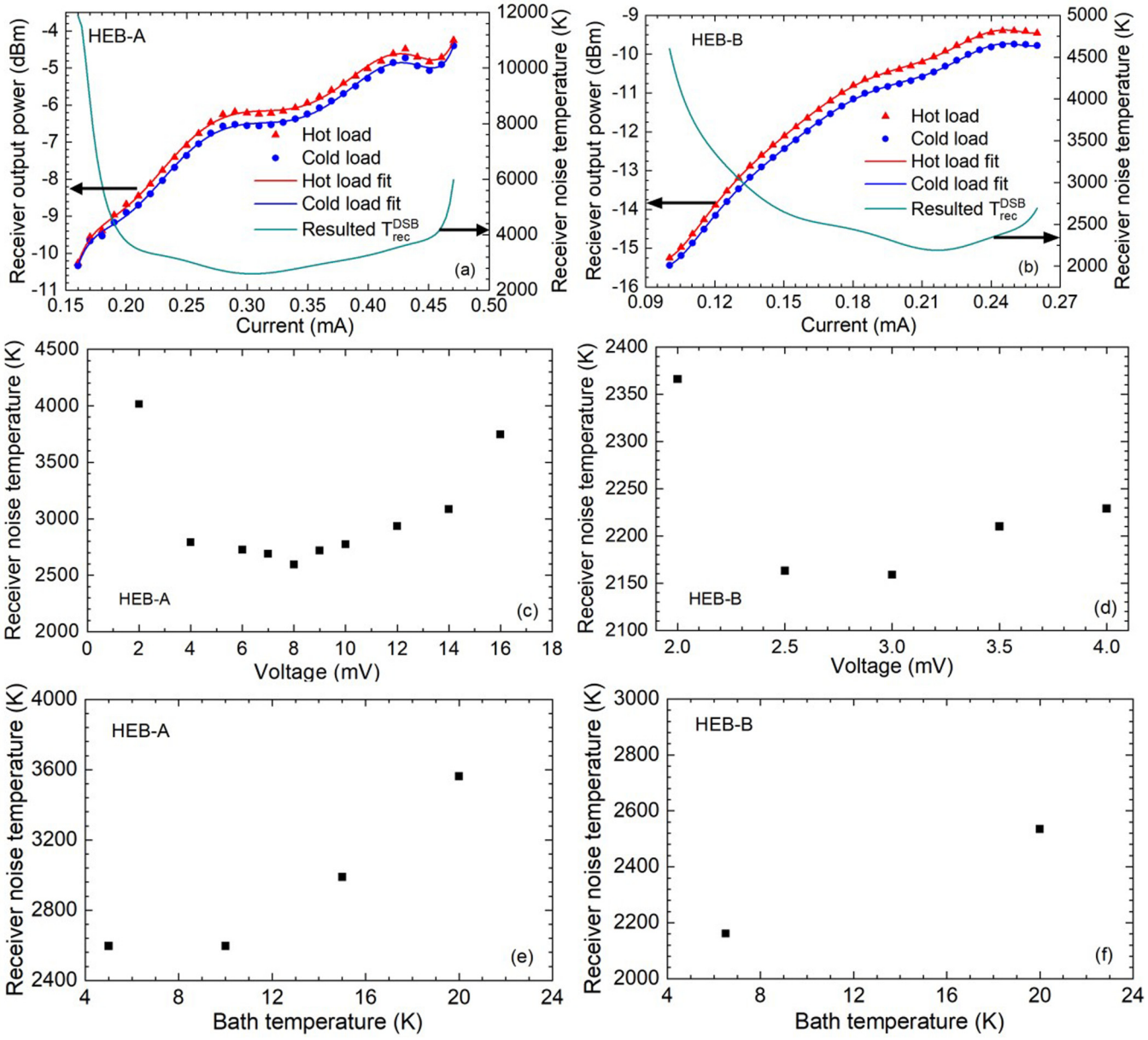

FIG. 5. (a) and (b) Measured receiver output power (left axis) of HEB-A (biased at 8 mV) and HEB-B (biased at 2.5 mV), respectively, in response to hot/cold loads, together with the polynomial fits (solid lines) as a function of the current and the resulting receiver noise temperature (right axis) when it is operated with an LO at 1.6 THz. The lowest noise temperature for HEB-A is 2590 K and for HEB-B is 2160 K. (c) and (d) The minimum receiver noise temperatures of HEB-A and HEB-B for different bias voltages. (e) and (f) The minimal T_{rec}^{DSB} at different operating (bath) temperatures. Results of HEB-A are for f_{if} = 2 GHz (Δf_{if} = 100 MHz), while those of HEB-B are for f_{if} = 1.7 GHz (Δf_{if} = 85 MHz).

C. Receiver noise temperature vs bias voltage at 1.6 THz

We measured P_{hot} and P_{cold} of both HEBs as a function of the bias voltage under the optimally pumped LO power. The results from HEB-A are plotted in Fig. 6, where the P_{hot} and P_{cold} show irregular features that are also present in the resulting T_{rec}^{DSB}. The latter is plotted in the same figure in green. The irregular features are reproducible, but some details seem to vary, probably due to fluctuations in the LO power from the FIR gas laser. For this

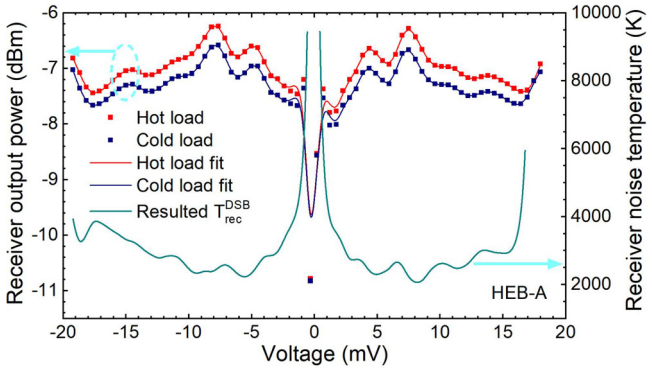

FIG. 6. Measured receiver output power (left axis) of HEB-A responding to the hot and cold load and resulting T_{rec}^{DSB} (right axis) as a function of the bias voltage with the HEB pumped at the optimal LO power at 1.6 THz and at 5 K operating temperature. Solid lines for the receiver output power are smoothed curves.

particular measurement (as a function of the bias voltage), we were not able to keep the LO power constant. The T_{rec}^{DSB} as a function of the bias voltage for HEB-A shows a minimum T_{rec}^{DSB} of 2070 K at 8 mV, which is 20% lower than what is found in Fig. 5(a). This is caused by LO power variation between the measured hot and cold power curves.

To understand the structure of $P_{hot,cold}$, we measured the $P_{hot,cold}$ of HEB-B as a function of bias voltage within a relatively short time period by scanning a relatively small voltage range (0–5 mV) with a voltage step (0.1 mV), so the LO power was relatively constant and the data, which are reproducible, are chosen to be discussed further. The dataset was taken from the same HEB although at 5.3 THz and 20 K instead of 1.6 THz and 5 K, which should not affect the discussion. Figure 7 plots the IV curves and $P_{hot,cold}$ and T_{rec}^{DSB} vs V, respectively. The two identical IV curves in Fig. 7(a) indicate that the LO power is the same when measuring P_{hot} and P_{cold}. The curves of $P_{hot,cold}$ in Fig. 7(b) show clearly structures, which are expected to correlate to the structures in the curves of dV/dI vs V, to be discussed. The derived T_{rec}^{DSB} curve in Fig. 7(c) shows also structure, which is interestingly not fully in line with the peaks and valleys in the $P_{hot,cold}$ curves. It is worth to note that the variation in amplitude is much larger than the uncertainty of the measurement data.

We believe the structure in the $P_{hot\ or\ cold}$ vs V curve originates from the IV or the differential resistance dV/dI vs V. However, the IV curves in Fig. 7(a) with the large voltage step do not allow us to calculate the small features in dV/dI due to the noise. By smoothing the data, the main fluctuating features are averaged out. Instead, we plot the dV/dI of the same HEB (HEB-B) as a function of bias voltage over a wide voltage range from 0 to 40 mV for an optimally pumped case (at 1.6 THz) together with P_{hot} in Fig. 8, where we found that the large features in the dV/dI curve correspond well to those in the P_{hot} curve. We conclude that the structure on P_{hot} correlates to the differential resistance.

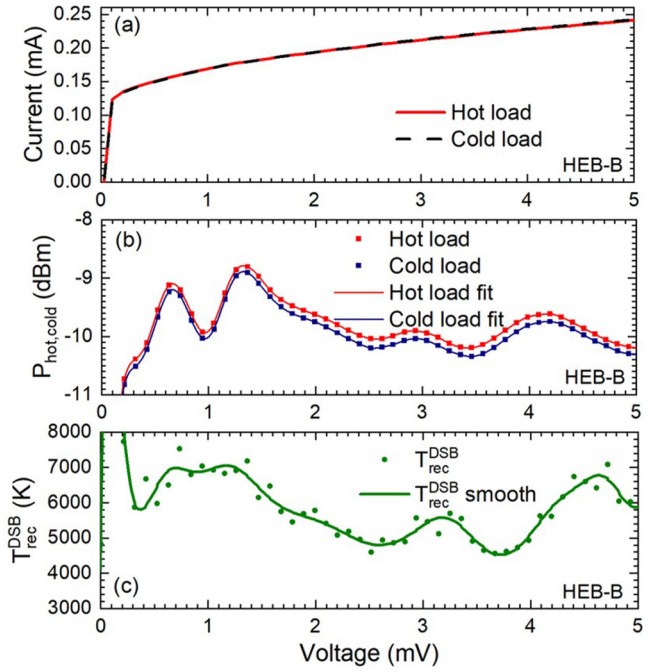

FIG. 7. Measured results for HEB-B when it was pumped at the optimal LO power at 5.3 THz and at 20 K operating temperature. (a) Measured IV curves with the HEB responding to the hot or cold load; (b) measured receiver output power responding to the hot or cold load as a function of the bias voltage; (c) DSB receiver noise temperature, T_{rec}^{DSB}, as a function of the bias voltage derived from the Y-factor based on $P_{hot,cold}$ data in (b).

D. Receiver noise temperatures at 2.5 THz

We also measured the T_{rec}^{DSB} of HEB-A with the LO at 2.5 THz. Using the same current scan method, we obtained a minimum T_{rec}^{DSB} of 3290 K at 8 mV and 0.31 mA. The details are illustrated in

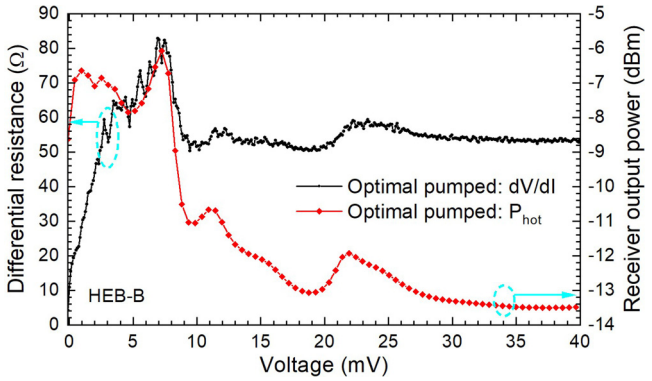

FIG. 8. Comparison between the measured receiver output power P_{hot} and the differential resistance of HEB-B (from IV) as a function of the bias voltage with the HEB pumped at the optimal LO power at 1.6 THz and at 5 K operating temperature.

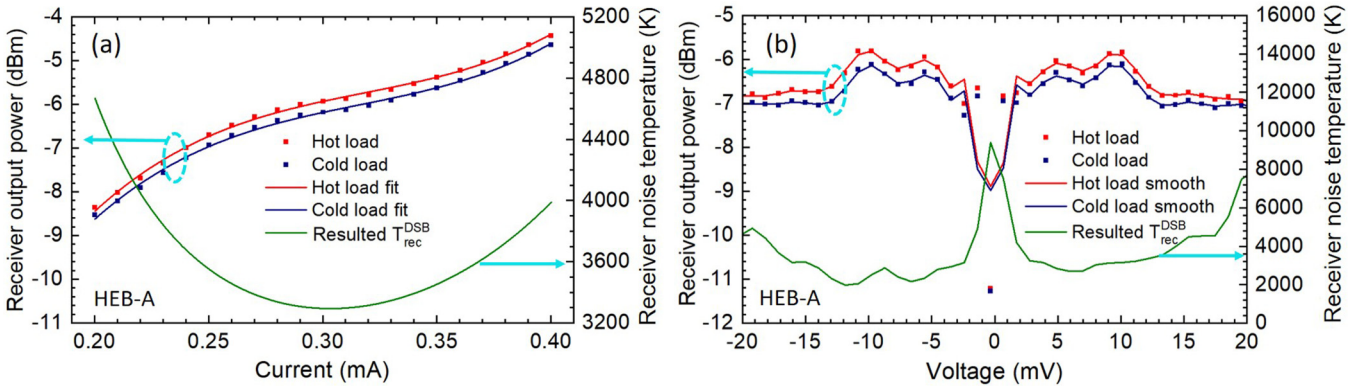

FIG. 9. (a) Receiver output power (left axis) and resulting T_{rec}^{DSB} (right axis) as a function of HEB current at 5 K and 2.5 THz. Solid lines are polynomial fits. The minimum noise temperature is 3290 K at 0.31 mA. (b) Receiver output power (left axis) responding to the hot and cold load and resulting T_{rec}^{DSB} (right axis) as a function of the bias voltage with the HEB pumped at the optimal LO power at 2.5 THz and 5 K. The solid lines for the receiver output power are the curves as a result of smoothing.

Fig. 9. By increasing the LO frequency to 2.5 THz, the optical losses in the optical path are also increased, as shown in Table III; in particular, there is more loss at the AR-coated Si lens because it was optimized for 1.6 THz. To establish a sensitivity of the MgB_2 HEB at 2.5 THz, we also calculated the receiver noise temperature referred to the front of the Si lens by correcting the optical losses of the components in the optical path before it (lens) and by assuming an AR-coated lens optimized for the right frequency. We found this corrected T_{rec}^{DSB} to be 1866 K. The latter is about 14% higher than the corrected T_{rec}^{DSB} value at 1.6 THz (to be described in Sec. V A). The structure was also observed in P_{hot} and P_{cold} vs voltage at 2.5 THz.

E. IF noise bandwidth

Sections IV B–IV D present our studies of the MgB_2 HEB mixer sensitivity (T_{rec}^{DSB}) in a narrow (100 MHz or 85 MHz) band, centered at f_{if} =2 GHz or f_{if} =1.7 GHz. In practical astronomical observations, different IFs are utilized, depending on how far the LO frequency is from the frequency of the celestial source. Furthermore, as we discussed in the Introduction, an IF band as wide as several GHz is often required.[3] Wide-IF-band characterization of T_{rec}^{DSB} with a high frequency resolution will also provide insight into the physics of HEB mixers and determine their time response limits associating to the ultra-thin MgB_2 films used.

With this goal in mind, device HEB-A was studied across a wide IF range of 0.2–14 GHz when the HEB is biased at the optimal point at 5 K and with the 1.6 THz LO. The obtained T_{rec}^{DSB} is plotted as a function of IF frequency in Fig. 10(a). We used the equation $T_{rec}^{DSB}(f) = T_0(1 + (f/f_n)^2)$ to fit the T_{rec}^{DSB} vs IF data. For this device, we have the best fit when the NBW is 11 ± 1 GHz, where the large error bar is due to the low signal-to-noise ratio. The IF NBW of HEB-B (with an uncoated lens for this particular measurement) were also fitted and measured to be 11 ± 1 GHz, as

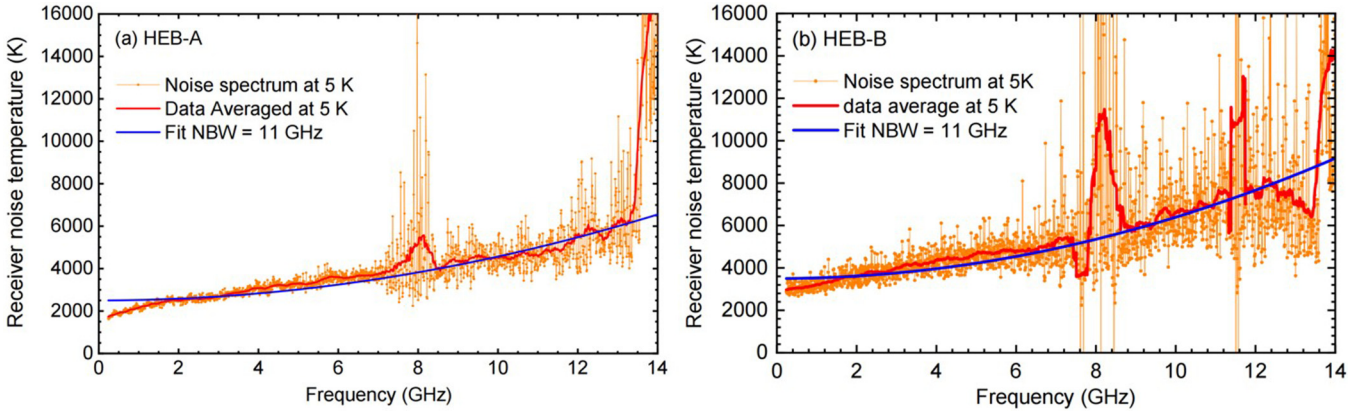

FIG. 10. T_{rec}^{DSB} as a function of IF frequency at 5 K and 1.6 THz for device HEB-A in (a) and device HEB-B (with uncoated lens) in (b). The solid lines are the fits to the data using the equation $T_{rec}^{DSB}(f) = T_0(1 + (f/f_n)^2)$, and the fitted noise bandwidth f_n for both devices are 11 GHz with an error bar of ±1 GHz.

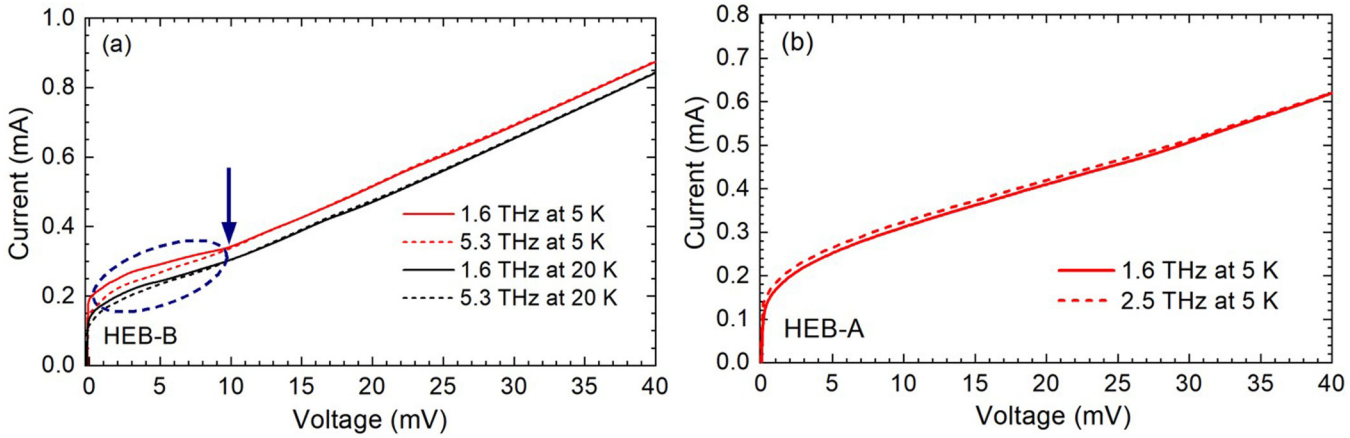

FIG. 11. Comparison of the IV curves at two different frequencies for both MgB_2 HEBs. (a) The optimally pumped IVs at 1.6 and 5.3 THz for HEB-B, at 5 and 20 K. Reproduced from Gan *et al.*, Appl. Phys. Lett. **119**, 202601 (2021). Copyright 2021 AIP Publishing LLC. (b) The optimally pumped IVs at 1.6 and 2.5 THz at 5 K for HEB-A.

shown in Fig. 10(b). Our NBW data support the results reported in Refs. 32 and 47.

An unexpected peak in the T_{rec}^{DSB} vs IF is observed at 8 GHz (and at 12 GHz for HEB-B) at all temperatures, operating points, and LO frequencies. It is also seen in data for different HEBs. Characterization of each IF component separately does not allow us to see where this particular problem could be. It seems to come from an interaction of the HEB mixer itself with the extremely broadband IF LNA that we utilized. A study of the IF impedance of MgB_2 HEB mixers is required for an accurate HEB-to-LNA integration. Fortunately, this peak has little effect on our determination of the NBW because of the wide IF range used.

F. Comparison of pumped IV at different frequencies

For HEB-B, we measured its optimally pumped IVs at 1.6 and 5.3 THz at both 5 and 20 K, which are plotted in Fig. 11(a). A presence of the bulging part in the IV roughly below 10 mV at 1.6 THz (indicated with an arrow) as compared to the IV at 5.3 THz is characteristic to this device. However, the difference, the increased current at 1.6 THz in this region compared to 5.3 THz, vanishes as the voltage increases. The two IV curves become exactly the same at high voltages, where the HEB turns into a resistive state toward the normal state. Since in this case the effective gap frequencies are substantially reduced, the absorption of photon power is expected to be no longer dependent on the photon frequency. The well-overlapping IV curves at high voltages suggest the same LO power at 1.6 and 5.3 THz. We note that the effect is also present at 20 K but weaker.

For HEB-A, we have measured its optimally pumped IVs at 1.6 and 2.5 THz at 5 K, which are plotted and compared in Fig. 11(b). We found they are almost identical. The slight offset in the currents is due to a small difference in LO power. Physical interpretations of the observations in both HEBs, taking the double-gap nature into account, will be discussed in Sec. V C.

V. DISCUSSION

A. Comparison of the measured receiver noise temperatures with other HEBs

The measured T_{rec}^{DSB} of 2160 K at 1.6 THz for HEB-B is promising and better than other MgB_2 HEBs reported in the literature,[29–31] where although the operating frequencies and detailed optics are not the same, this general conclusion is valid. However, our value is higher than the best MgB_2 HEB in Ref. 32. To compare with the data in Ref. 32, we corrected for optical losses until the front of the AR-coated Si lens in the same way as what was done in Ref. 32, and we find a value of 1634 K in our case. This value is 1.6 times higher than ~1000 K derived from Ref. 32. We continue the comparison by listing G_m^{DSB}, which is −7.8 dB for HEB-B and −6.2 dB for MgB_2 HEB in Ref. 32. The factor of 1.6 is largely explained by the difference in G_m^{DSB}. We notice that HEB-B has a narrower MgB_2 bridge of 285 nm, while the HEB in Ref. 32 has a bridge width of 1 μm. As demonstrated in Ref. 49, the T_{rec}^{DSB} increases with reducing the bridge width. This might explain the difference. We could confirm this by measuring a wider HEB. Unfortunately, the LO power is not sufficient to optimally pump the larger HEB.

Since we determined experimentally G_m^{DSB} for HEB-B, we can also derive its minimum T_{mix}^{DSB} at 1.6 THz in the same way as in Ref. 34, which is 1319 K and is also included in Table IV.

Our best T_{rec}^{DSB} at 1.6 THz is 3–4 times the T_{rec}^{DSB} found in a NbN HEB measured in a very similar vacuum setup, after correcting for losses in the uncoated Si lens (842 K on an uncoated Si lens).[36] The higher noise temperature in MgB_2 HEB due to the high T_c is expected because the output noise is proportional to it.[50] However, the mixer conversion gain might be different from the NbN HEB and is expected to be higher. As shown in Sec. IV B, HEB-B has a G_m^{DSB} of −7.8 dB, which is higher than −9.47 dB found for the NbN HEB in Ref. 36. Our recent, unpublished results[51] have also shown that NbN HEBs can have a higher G_m^{DSB},

e.g., −3.2 dB at 1.6 THz. As a result, the T_{rec}^{DSB} was also reduced considerably, for example, to 490 K. Therefore, we believe that the G_m^{DSB} of MgB_2 HEBs can be further improved and, thus, T_{rec}^{DSB}.

The T_{rec}^{DSB} increases by 37% for HEB-A and 17% for HEB-B when the mixer operating temperature increases from 5 to 20 K. Compared to the 12% increase in T_{rec}^{DSB} for HEB-B operated at 5.3 THz,[34] the increase in T_{rec}^{DSB} for HEB-B at 1.6 THz is slightly higher. The reason could be the different electron temperature profiles of the device due to the different LO frequencies, caused by the double gap effect to be discussed in Sec. V C, which causes a different temperature dependence of T_m^{DSB} and, thus, T_{rec}^{DSB}. The MgB_2 HEB has the advantage of operating at temperatures ≥20 K, but the degradation with increasing temperature depends on T_c; thus, HEB-B is more favorable for 20 K operation. Uniquely, between 5 and 10 K, the sensitivity is nearly temperature independent.

B. Origin of the structure in IV, output power, and receiver noise temperature

The stepwise features appearing in the IV curves of narrow- or nano-wires based on an ultrathin MgB_2 film are known in the literature. Such MgB_2 nanowires can show current jumps and discontinuities in their IV curves.[52] The nanowire in Ref. 52 has a width of 320 nm based on a 10 nm thick film, which is very comparable to our HEBs. The amplitude of the stepwise features depends on temperature. By raising the temperature, the IV curve gradually becomes smooth and the structure seems to be washed out, but it might still be present since no differential resistance data were shown. The latter can magnify the detailed features. Such data were obtained when the devices are current biased. However, in our case, all the IV curves were recorded when the HEB is voltage biased, where the bias circuit can influence the detailed features. Because of this, our HEBs are not expected to show exactly the same features as in Ref. 52.

Fine features in the differential resistance of the pumped IV under THz radiation have been observed in an MgB_2 HEB geometry,[31] where fluctuations are observed in the receiver output power of the HEB vs the voltage. The authors attributed them to sudden switches in the resistance. However, little discussion on the origins can be found. The irregular features observed in the IV curves or their differential resistance vs voltage are expected to relate to the film quality, the transport mechanism, or a combination of both. It was reported that a thin MgB_2 film of 40 nm grown by HPCVD shows well-connected hexagonal grains with sizes ranging from 90 to 180 nm,[21] where the electrical connectivity between the grains is expected to be weak when the film gets thinner. Since the grain sizes vary in the film, one could expect electronic inhomogeneities intrinsic to grains in MgB_2 thin films, where there are spatial variations in the critical temperature and where the effect to the IVs is magnified in the bridges with a submicrometer-width.

Unfortunately, we have no information of the material and surface structure of our specific MgB_2 HEBs. So we do not know whether the mechanism of the grains in the electrical transport is applicable to our case. However, we find that a comparable MgB_2 film of 5 nm thick (nominal) has shown considerable fluctuations of the surface profile, measured by an atomic force microscopy (AFM) scan, where local peaks or dips reach an amplitude of as much as 3 nm in a scale of roughly 100 nm spatially. So the film uniformity is absolutely not ideal because the fluctuation amplitude is close to the thickness. We thus expect strong non-uniform electronic properties, which result in spatial variations in the critical temperature. As suggested in Ref. 53, local variations in the critical temperature in NbTiN narrow strips can cause stepwise features in IV curves. This mechanism may also apply to our narrow MgB_2 bridges.

By applying a hotspot mixing mechanism[54,55] to an uniform HEB, one will derive structure-less $P_{hot,cold}$ and T_{rec}^{DSB} vs V curves although they are voltage dependent and although there is a minimal T_{rec}^{DSB} at the optimal bias voltage as shown in NbN HEBs.[11,40] However, the non-uniform electronic properties can introduce an additional structure in addition to the voltage- and LO power dependence governed by the hotspot. Thus, $P_{hot,cold}$ will also show structure, where the location and amplitude of peaks and valleys will be both voltage and LO power dependent. In essence, the mixer gain and output noise will be affected by the non-uniformity. As a result, the MgB_2 HEBs can have reproducible structure in $P_{hot,cold}$ and T_{rec}^{DSB}. In contrast to a NbN HEB, the non-uniform MgB2 HEB can have different local minimal noise temperatures, as demonstrated in Fig. 7(c).

It has not been studied yet whether the additional structure can influence the direct detection effect[56] or the stability[57] of the HEB. But we noticed that LO power needs to be absolutely constant between two measured traces of $P_{hot,cold}$ of the HEB as a function of bias voltage; otherwise, the features in the output power curve change, for example, P_{hot} curve will shift with respect to the P_{cold} one. As a result, additional fluctuation features appear in the T_{rec}^{DSB}, making the measured values less reliable.

C. Effect of the gap frequency

$\Delta_\pi = 1.8$ meV and $\Delta_\sigma = 6.3$ meV were reported for MgB_2 with a T_c of 38.7 K,[58] corresponding to gap frequencies, f_π *and* f_σ, of 0.87 and 3.05 THz, respectively. The two frequencies are derived by making use of the relation of the gap frequency to the superconducting gap of π-band or σ-band, namely, $f_\pi = 2\Delta_\pi/h$, while $f_\sigma = 2\Delta_\sigma/h$,[18] where h is the Planck constant. We assume that these two gap frequencies apply also to HEB-B since its T_c (38.4 K) is nearly the same as in Ref. 58. Actually recently, Ref. 59 has found comparable two gap frequencies by measuring the kinetic inductance of a similar thin film. Photo-response in double energy gap superconductors is an interesting research problem itself and deserves a separate study. Nevertheless, since the frequencies of LO sources utilized in our experiments occur on both sides of f_σ, and since LO power has been known to affect the shape of the pumped IVs, we took this opportunity to verify whether the double-gap conduction bands in MgB_2 could be manifested in MgB_2 HEBs by the LO frequency.

Pumped IVs of HEBs are a result of RF heating by THz radiation and dc heating by the current in the superconducting bridge. A resistance over a hot-spot, which appears in the middle of the HEB, is observed as the voltage in the IVs under both the LO and the dc-voltage (current) bias. Obviously, if f_{LO} *is* $< 2\Delta/h$, the LO photons can be absorbed only in the areas with a suppressed

energy gap. In case $f_{LO} > 2\Delta/h$, the LO photons are absorbed uniformly within the HEB. This phenomenon was indeed observed experimentally in low-T_c superconducting NbN HEBs when the LO frequency varies across its gap frequency.[60,61] Furthermore, with a gap frequency of $2\Delta/h$ at ~0.8 THz, the IV curves of a NbN HEB show no variations vs LO frequency from 1.6 up to 5.3 THz.[36]

Photons of 5.3 THz are expected to break Cooper-pairs uniformly within the ultrathin, narrow MgB_2 bridge since $f_\sigma < 5.3$ THz. However, when it is pumped at 1.6 THz, which is expected to be between f_π and f_σ, the photons can break the Cooper-pairs in the π-band and only those in σ-band, which are located in the middle of the bridge, i.e., in the hot-spot created by the DC heat power. Thus, for the considered case ($f_\pi < 1.6\,\text{THz} < f_\sigma$), the absorption is highly non-uniform. Figure 11(a) shows IV curves for HEB-B pumped both at 1.6 and 5.3 THz at both 5 and 20 K. At both temperatures, the following relation is valid: $f_\pi < 1.6\,\text{THz} < f_\sigma < 5.3\,\text{THz}$. It is clear that at the high bias voltages, when the superconductivity is suppressed and the hot spot extends over the entire HEB, the effect of the LO frequency cannot be observed. On the contrary, at lower bias voltages [in Fig. 11(a)], a clear reduced effect of LO power heating on the HEB (a higher current for a given bias voltage) at 1.6 THz is seen. This effect, as one would expect, is stronger at 5 K than at 20 K due to a marginally reduced energy gap in the latter case, but the relation $f_\pi < 1.6\,\text{THz} < f_\sigma < 5.3\,\text{THz}$ is still valid, while the two IV curves are exactly the same at voltages from roughly 10 to 40 mV. The latter suggests that the pumped LO power is the same since the pumped IV curves are still LO power dependent as indicated in Fig. 4. This observation can be explained by the existence of a high-energy σ-band with a characteristic frequency between 1.6 and 5.3 THz in the FIR absorption spectrum of MgB_2 films. We are unfortunately not able to probe the small π-gap since we have not measured the IV pumped with a LO frequency below f_π of 0.87 THz.

How the double-gap absorption of the photons from the LO will affect the MgB_2 HEB performance has to be modelled using, e.g., a finite element modeling, which will require knowledge of many superconducting parameters of the utilized films. At the moment, we can state that the measured G_m^{DSB} at 1.6 THz (−7.8 dB) for our MgB_2 HEB is found to be slightly lower than that at 5.3 THz (−6.7 dB). This difference from 1.6 to 5.3 THz is small but noticeable (+1.1 dB). In contrast, the G_m^{DSB} of an NbN HEB is known to be nearly constant although decreasing slightly (−0.4 dB) from 1.6 to 5.3 THz in practice.[36]

Although the film used for HEB-B is much thinner (~7 nm) than the one reported in Ref. 20, which is 200 nm, it has a relatively high T_c of 38.4 K and a low room temperature resistivity (~22 $\mu\Omega \times$ cm), hence being close to the clean limit. The cleanness is attributed to the thick Si_3N_4 protection layer, which prevents MgB_2 from being exposed to moisture in the air.

HEB-A does not show similar behavior in the pumped IV between 1.6 and 2.5 THz as HEB-B. Thus, no signature of the high-energy gap is present. The reason is unclear. Likely, the MgB_2 bridge without a protection layer in HEB-A is considered to be "dirty" because the MgB_2 has been in contact with moisture and is, thus, hard to observe the high-energy gap, as reported in Ref. 22.

D. RF impedance of a MgB_2 HEB

Section V C implies that to explain the RF performance of an MgB_2 HEB, like HEB-B, one needs to be aware of the operating frequency with respect to two gap frequencies. Let us here discuss what will be the RF impedance of an MgB_2 HEB at different frequencies. For the case of HEB-A, the RF impedance could be considered to be the same as the normal resistance just above its T_c when we apply the LO frequency at 1.6 and 2.5 THz since both are considerably higher than the assumed single gap frequency of 1.2 THz corresponding to a Δ_π of 2.5 meV as suggested in Ref. 22. Also the HEB film thickness is less than 25% of the skin depth (δ) of 142 nm (at 1.6 THz) of the MgB_2 at its normal.[62] Furthermore, since the δ is about 36% of the HEB width, the RF current will be uniform along the MgB_2 HEB since this is very similar to the NbN HEB with Au contact pads in Ref. 63, where the current distribution is constant across the HEB width even when δ/HEB width is 17% at 8 THz. NbN HEB mixers are often within this limit; thus, for a NbN HEB operated beyond 1 THz, the RF impedance is usually taken from the normal state resistance.

However, the RF impedance for HEB-B will depend on the LO frequency, either 5.3 or 1.6 THz. At 5.3 THz, the impedance will be the same as the normal state resistance since it is far above the two gap frequencies, and the HEB thickness is far less than 25% of the δ of 75 nm of MgB_2. Furthermore, δ is 26% of the HEB width.[63] In contrast, at 1.6 THz, it is a frequency between two gap frequencies, so for the σ-band conduction, it is still superconducting, while for π-band conduction it behaves like normal. Thus, the impedance needs to be calculated by using the general complex surface impedance for a superconducting film under AC in a similar approach as for a NbN HEB when it is operated below its gap frequency.[61,64] One more complication is that when it is DC biased and LO pumped, the exact RF impedance could be operating point dependent. So, strictly speaking, for HEB-B, the RF impedance at 1.6 THz is not known, but is likely smaller than the normal state resistance. Thus, the power coupling between the HEB and antenna shown in Table IV is just an approximation since it was based on the normal state resistance.

E. R–T curves and contacts

It is surprising to notice that two HEBs from different batches have shown the R–T curves in Fig. 1(c) that seem to be fully characterized by only one T_c, namely, the T_c of the thin MgB_2 films. In contrast, both NbN HEB[65] and Nb HEB,[66] contacted commonly with thick Au pads being the same as for the MgB_2 HEBs, have shown not only a reduced T_c of contact pads, which consist of a superconducting layer and an Au layer, but also a slow increase in resistance from the T_c of the contacts. Here, we focus only at one particular phenomenon that is the reduced T_c of NbN/Au or Nb/Au contacts,[65,66] which is known to be caused by the superconducting proximity effect. The latter describes a leak of Cooper pairs from a superconductor (S) into a normal metal (N) when they are in contact physically. For a given N, the parameters of superconducting coherence length (ξ), the thickness in the superconductor d_s, and the transparency of the interface between S and N play a crucial role to determine the leaking distance of Cooper pairs in the S–N structure[67] and, in turn, to determine the reduced T_c of

the S–N layer. To examine possible proximity effects in our MgB_2–Au bilayer, we compare the parameters of ξ and d_s out of three types of HEBs. We find ξ, the coherence length ξ_c along the c-axis for thin MgB_2 films, to be 2–3 nm[68] and $d_s = 5$–7 nm in our case, while ξ is 3–4[65] and $d_s = 5$–6 nm for NbN films (in practice), and ξ is 5 nm for Nb films[69] and $d_s = 10$ nm. We observe that the ratio, ξ/d_s, for MgB_2 is comparable to that for NbN in magnitude, although MgB_2 is expected to have a slightly weaker proximity effect. Furthermore, it has been shown that MgB_2 is a phonon-mediated BCS superconductor,[70] which should behave similarly as Nb and NbN but operate at a higher temperature. Therefore, if the interface between S and N is transparent, one should expect the proximity effect also from the MgB_2/Au structure. The observation of no reduction in T_c in our MgB_2/Au contact pads suggests that the interface between MgB_2 and Au is poor. If this is true, improving the interface may further improve the performance of MgB_2 HEB mixers. The existence of poor contacts or the contact resistance in MgB_2 HEBs was suggested by the measured dependence of mixer noise temperatures on the bridge width, where the mixer noise temperature is lower when the width is larger.[49]

F. Preventing aging effect

HEB-A and other devices (not shown) from the same batch suffered from an aging effect, where the R_N increases with time and shows more changes when we removed the HEB from the Si lens, in which the HEB is usually exposed to moisture in the air. However, HEB-B and other devices with the protection layer have shown no changes in R_N although HEB-B has been exposed to moisture more than 5 times during a 2-month measurement campaign. Thus, the protection layer is crucial, not only preserving the transport property by keeping the resistance of the HEB unchanged, but also maintaining it in the clean limit. We also stored two HEBs from the same batch as HEB-B in air and monitored the R_{RT} as a function of time for a period of 400 days. We measured a relative change of 0.7% in the resistance averaged from two HEBs, which is negligibly small. Even so, we keep such HEBs in a storage in vacuum, so the aging effect can be mitigated to almost zero.

VI. CONCLUSIONS

We have fabricated spiral antenna-coupled MgB_2 hot electron bolometer mixers based on ultrathin MgB_2 films of ∼5 nm, corresponding to a T_c of 33.9 K, and ∼7 nm, corresponding to a T_c of 38.4 K. At 1.6 THz, we measured a minimal DSB receiver noise temperature (T_{rec}^{DSB}) of 2590 K for HEB-A using a standard setup in air and 2160 K for HEB-B using a vacuum setup. After correcting for differences in optical losses between the two setups, both HEBs show a comparable T_{rec}^{DSB}. We realized HEB mixers with narrower MgB_2 bridges than in Refs. 32 and 47 where the best values so far were ∼1000 K, referenced to the front of the AR-coated Si lens. In our case, this value is 1634 K for HEB-B. We believe that the difference is due to contact resistance between the Au contact pads and the MgB_2 bridge, where the effect is larger for narrower bridges. All the T_{rec}^{DSB} are measured around an operating temperature of 5 K, with a local oscillator power of 13.6 μW for HEB-A and 12.5 μW for HEB-B. The IF noise bandwidths for both HEB-A and HEB-B were measured to be 11 GHz, which agree with the data in Refs. 32 and 47, and are roughly three times larger than what was found for NbN HEBs. When the operating temperature increases from 5 to 20 K, T_{rec}^{DSB} at 1.6 THz increases by 37% for HEB-A and only 17% for HEB-B, confirming a high operating temperature above 20 K, especially for HEBs with higher critical temperatures (38 K in our case).

We measured a minimal T_{rec}^{DSB} of 3290 K at 2.5 THz and at 5 K using HEB-A, leading to a corrected T_{rec}^{DSB} of 1866 K. The results obtained at 2.5 THz together with the recent data in Ref. 35 represent the first reported noise data at this frequency for an MgB_2 HEB in the literature, which adds to the understanding of the complex THz-response nature of double-gap MgB_2 HEBs.

We have observed the structure in the IV curves, which becomes weaker when the LO power increases, and can be observed only in their differential resistance in optimally pumped IVs. The structure is likely due to spatial variation in the thickness of the ultrathin MgB_2 films, which leads to spatial variation in the critical temperature. The effect on IV curves is magnified in narrow, submicrometer bridges. We also found the structure in the output power of the mixer as a function of bias voltage, which correlates with that in the differential resistance and also in the measured receiver noise temperature. They are reproducible, but sensitive to LO power. So, to determine a reliable T_{rec}^{DSB} as a function of the bias voltage, stable LO power is a must.

Different response in the IV curves around low bias voltages, pumped with the same power at either 1.6 or 5.3 THz, was observed for HEB-B, suggesting the presence of a high-energy gap in the ultrathin MgB_2.

Our studies suggest how to (a) further improve MgB_2 HEBs, including the structure in the IV curves being associated with the thin MgB_2 film requires an in-depth study before this technology can be fully implemented in a practical receiver; (b) characterize the stability of MgB_2 heterodyne receivers in terms of an Allan variance stability time,[57,41] in particular, to explore whether the structure appearing in the IV curves affects the stability or not; (c) understand the interface between Au and MgB_2, it is crucial to reduce the contact resistance, thus allowing not only for a better sensitivity, but also to have HEBs with a small width and, thus, smaller HEBs. The latter allows for operating at a low LO power, which facilitates array receivers. Finally, to predict the ultimate heterodyne performance of MgB_2 HEBs, detailed modeling, as performed for NbN and YBCO HEBs, would be extremely valuable.

ACKNOWLEDGMENTS

We thank J. Chang for his supports to the fabrication of MgB_2 devices; P. Khosropanah and A. Aminaei for their advices on IF circuitry; and W. Laauwen, W.-J. Vreeling, B. Kramer, H. Ode, and R. C. Horsten for their valuable technical support. The work at Chalmers University of Technology was supported by the Swedish Research Council (No. 2019-04345) and the Swedish National Space Agency (No. 198/16). The work at TU Delft was partly supported by the TU Delft Space Institute (DSI). Y.G. also thanks J. G. bij de Vaate for supporting her Ph.D. activity within the Instrument Science Group at SRON. Y.G. was funded partly by the

China Scholarship Council (CSC) and partly by the University of Groningen.

AUTHOR DECLARATIONS

Conflict of Interest

The authors have no conflicts to disclose.

Author Contributions

Y. Gan: Conceptualization (equal); Data curation (lead); Formal analysis (lead); Investigation (lead); Methodology (lead); Project administration (lead); Software (lead); Validation (lead); Visualization (lead); Writing – original draft (lead); Writing – review & editing (equal). **B. Mirzaei:** Data curation (equal); Investigation (equal); Methodology (equal); Project administration (equal); Validation (equal); Visualization (equal); Writing – review & editing (equal). **J. R. G. Silva:** Data curation (supporting); Formal analysis (supporting); Methodology (supporting); Visualization (supporting); Writing – review & editing (supporting). **S. Cherednichenko:** Resources (supporting); Visualization (supporting); Writing – review & editing (supporting). **F. van der Tak:** Project administration (supporting); Resources (supporting); Supervision (equal); Writing – review & editing (supporting). **J. R. Gao:** Conceptualization (equal); Funding acquisition (equal); Resources (equal); Supervision (equal); Writing – review & editing (equal).

DATA AVAILABILITY

The data that support the findings of this study are available from the corresponding author upon reasonable request.

REFERENCES

[1]E. M. Gershenzon, G. N. Gol'tsman, I. G. Gogidze, Y. P. Gusev, A. I. Elant'ev, B. S. Karasik, and A. D. Semenov, "Millimeter and submillimeter range mixer based on electron heating of superconducting films in the resistive state," Sov. Phys. Supercond. **3**(10), 2413–2160 (1990).
[2]H.-W. Hubers, "Terahertz heterodyne receivers," IEEE J. Sel. Top. Quantum Electron. **14**, 378–391 (2008).
[3]F. F. S. van der Tak, S. C. Madden, P. Roelfsema, L. Armus, M. Baes, J. Bernard-Salas *et al.*, "Probing the baryon cycle of galaxies with SPICA Mid- and far-infrared observations," Publ. Astron. Soc. Aust. **35**, E002 (2018).
[4]C. Risacher, R. Gusten, J. Stutzki, H.-W. Hubers, D. Buchel, U. Graf *et al.*, "First supra-THz heterodyne array receivers for astronomy with the SOFIA observatory," IEEE Trans. Terahertz Sci. Technol. **6**(2), 199–211 (2016).
[5]D. J. Hayton, J. L. Kloosterman, Y. Ren, T. Y. Kao, J. R. Gao, T. N. Klapwijk, Q. Hu, C. K. Walker, and J. L. Reno, "A 4.7 THz heterodyne receiver for a balloon borne telescope," Proc. SPIE **9153**, 91531R (2014).
[6]T. de Graauw, F. Helmich, T. G. Phillips, J. Stutzki, E. Caux, N. D. Whyborn *et al.*, "The herschel-heterodyne instrument for the far-infrared (HIFI)," Astron. Astrophys. **518**, L6 (2010).
[7]C. Walker, C. Kulesa, A. Young, W. Verts, J. R. Gao, Q. Hu, J. Silva, B. Mirzaei, W. Laauwen, J. Hesler, C. Groppi, and A. Emrich, "Gal/Xgal U/LDB spectroscopic/ stratospheric THz observatory: GUSTO," in Proceedings of the SPIE 12190, Millimeter, Submillimeter, and Far-Infrared Detectors and Instrumentation for Astronomy XI (SPIE, 2022), p. 121900E.
[8]J. V. Siles, J. Pineda, J. H. Kawamura, P. F. Goldsmith, P. N. Bernasconi, C. E. Groppi, J. O. Gundersen, L. D. Anderson, R. Assef, C. Battersby, L. I. Cleeves, K. K. Davis, T. Diaz-Santos, D. J. Hayton, R. Herrera-Camus, R. Klessen, W. D. Langer, C. Lisse, P. D. Mauskopf, I. Mehdi, J. R. Olson, L. Pagani, M. Roellig, N. Schneider, Y. Seo, and A. Tielens, "ASTHROS: The astrophysics stratospheric telescope for high spectral resolution observations at submillimeter-wavelengths," in Proceedings of the SPIE 11445, Ground-Based and Airborne Telescopes VIII (SPIE, 2020), p. 114453G.
[9]C. K. Walker, G. Chin, S. Aalto, C. M. Anderson, J. W. Arenberg, C. Battersby *et al.*, "Orbiting astronomical satellite for investigating stellar systems (OASIS): 'following water from galaxies, through protostellar systems, to oceans,'" Proc. SPIE **11820**, 118200O (2021).
[10]D. Rigopoulou, C. Pearson, B. Ellison, M. Wiedner, V. Ossenkopf Okada *et al.*, "The far-infrared spectroscopic surveyor (FIRSS)," Exp. Astron. Springer Link **51**(3), 699–728 (2021).
[11]J. L. Kloosterman, D. J. Hayton, Y. Ren, T. Y. Kao, J. N. Hovenier, J. R. Gao, T. M. Klapwijk, Q. Hu, C. K. Walker, and J. L. Reno, "Hot electron bolometer heterodyne receiver with a 4.7-THz quantum cascade laser as a local oscillator," Appl. Phys. Lett. **102**, 011123 (2013).
[12]Y. P. Gousev, G. N. Gol'tsman, A. D. Semenov, E. M. Gershenzon, R. S. Nebosis, M. A. Heusinger, and K. F. Renk, "Broadband ultrafast superconducting NbN detector for electromagnetic radiation," J. Appl. Phys. **75**, 3695–3697 (1994).
[13]D. M. A. Aminou, J. L. Bézy, R. Meynart, P. Blythe, S. Kraft, I. Zayer *et al.*, "Meteosat third generation (MTG) critical technology pre-development activities," Proc. SPIE **7474**, 747407 (2009).
[14]H. Linz, H. Beuther, M. Gerin, J. R. Goicoechea, F. Helmich, O. Krause *et al.*, "Bringing high spatial resolution to the far-infrared," Exp. Astron. **51**, 661–697 (2021).
[15]J. W. Waters, L. Froidevaux, R. S. Harwood, R. F. Jarnot, H. M. Pickett, W. G. Read *et al.*, "The earth observing system microwave limb sounder (EOS MLS) on the aura satellite," IEEE Trans. Geosci. Remote Sens. **44**(5), 1075–1092 (2006).
[16]I. Mehdi, J. V. Siles, C. Lee, and E. Schlecht, "THz diode technology: Status, prospects, and applications," Proc. IEEE **105**(6), 990–1007 (2017).
[17]R. G. Ladret, A. J. Kreisler, and A. F. Dégardin, "YBCO-constriction hot spot modeling: DC and RF descriptions for HEB THz mixer noise temperature and conversion gain," in IEEE trans," Appl. Supercond. **25**(3), 1–5 (2015).
[18]Y. Xu, M. Khafizov, L. Satrapinsky, P. Kus, A. Plecenik, and R. Sobolewski, "Time-resolved photoexcitation of the superconducting two-gap state in MgB_2 thin films," Phys. Rev. Lett. **91**, 197004 (2003).
[19]X. X. Xi, "Two-band superconductor magnesium diboride," Rep. Prog. Phys. **71**, 116501 (2008).
[20]M. Ortolani, P. Dore, D. Di Castro, A. Perucchi, S. Lupi, V. Ferrando, M. Putti, I. Pallecchi, C. Ferdeghini, and X. X. Xi, "Two-band parallel conductivity at terahertz frequencies in the superconducting state of MgB_2," Phys. Rev. B **77**, 100507(R) (2008).
[21]N. Acharya, M. A. Wolak, T. Tan, N. Lee, A. C. Lang, M. Taheri *et al.*, "Mgb_2 ultrathin films fabricated by hybrid physical chemical deposition and ion milling," APL Mater. **4**, 086114 (2016).
[22]R. A. Kaindl, M. A. Carnahan, J. Orenstein, D. S. Chemla, H. M. Christen, H.-Y. Zhai, M. Paranthaman, and D. H. Lowndes, "Far-infrared optical conductivity Gap in superconducting MgB_2 films," Phys. Rev. Lett. **88**, 027003 (2001).
[23]Y. Cui, J. E. Jones, A. Beckley, R. Donovan, D. Lishego, E. Maertz, A. V. Pogrebnyakov, P. Orgiani, J. M. Redwing, and X. X. Xi, "Degradation of MgB_2 thin films in water," IEEE Trans. Appl. Supercond. **15**, 224–227 (2005).
[24]K. Nakayama *et al.*, "Precise measurements of optical constants of SiC in 40 to 120 μm wavelength region," in *35th International Conference on Infrared, Millimeter, and Terahertz Waves* (IEEE, Piscataway, NJ, 2010), pp. 1–2. Note that the reflective index for SiC was found to increase slightly with increasing the frequency that is different from pure Si.
[25]M. Naftaly, J. F. Molloy, B. Magnusson, Y. M. Andreev, and G. V. Lanskii, "Silicon carbide—A high-transparency nonlinear material for THz applications," Opt. Express **24**, 2590–2595 (2016).
[26]S. Cherednichenko, V. Drakinskiy, K. Ueda, and M. Naito, "Terahertz mixing in MgB_2 microbolometers," Appl. Phys. Lett. **90**, 023507 (2007).

[27]S. Bevilacqua, E. Novoselov, S. Cherednichenko, H. Shibata, and Y. Tokura, "Mgb_2 hot-electron bolometer mixers at terahertz frequencies," IEEE Trans. Appl. Supercond. **25**(3), 1–4 (2015).
[28]E. Novoselov, S. Bevilacqua, S. Cherednichenko, H. Shibata, and Y. Tokura, "Effect of the critical and operational temperatures on the sensitivity of MgB_2 HEB mixers," IEEE Trans. Terahertz Sci. Technol. **6**(2), 238–244 (2016).
[29]D. Cunnane, J. H. Kawamura, M. A. Wolak, N. Acharya, T. Tan, X. X. Xi *et al.*, "Characterization of MgB_2 superconducting Hot electron bolometers," IEEE Trans. Appl. Supercond. **25**(3), 1–6 (2015).
[30]E. Novoselov, N. M. Zhang, and S. Cherednichenko, "Mgb_2 hot electron bolometer mixers for THz heterodyne instruments," Proc. SPIE **9914**, 99141N (2016).
[31]D. Cunnane, J. H. Kawamura, M. A. Wolak, N. Acharya, X. X. Xi, and B. S. Karasik, "Optimization of parameters of MgB_2 hot-electron bolometers," IEEE Trans. Appl. Supercond. **27**(4), 1–5 (2017).
[32]E. Novoselov and S. Cherednichenko, "Low noise terahertz MgB_2 hot-electron bolometer mixers with an 11 GHz bandwidth," Appl. Phys. Lett. **110**, 032601 (2017).
[33]N. Acharya, E. Novoselov, and S. Cherednichenko, "Analysis of the broad IF-band performance of MgB_2 HEB mixers," IEEE Trans. Terahertz Sci. Technol. **9**, 565–571 (2019).
[34]Y. Gan, B. Mirzaei, J. R. G. D Silva, J. Chang, S. Cherednichenko, F. van der Tak, and J. R. Gao, "Low noise MgB_2 hot electron bolometer mixer operated at 5.3 THz and at 20 K," Appl. Phys. Lett. **119**, 202601 (2021).
[35]C. A. Curwen, D. P. Cunnane, J. H. Kawamura, D. J. Hayton, and W. Yang, "THz heterodyne system using novel mixer and local oscillator devices," in *47th International Conference on Infrared, Millimeter and Terahertz Waves (IRMMW-THz)* (IEEE, Piscataway, NJ, 2022), pp. 1–2.
[36]W. Zhang, P. Khosropanah, J. R. Gao, E. L. Kollberg, K. S. Yngvesson, T. Bansal, R. Barends, and T. M. Klapwijk, "Quantum noise in a terahertz hot electron bolometer mixer," Appl. Phys. Lett. **96**, 111113 (2010).
[37]E. Novoselov, N. Zhang, and S. Cherednichenko, "Study of MgB_2 ultrathin films in submicron size bridges," IEEE Trans. Appl. Supercond. **27**(4), 1–10 (2017).
[38]Y. Zhang, Z. Lin, Q. Dai, D. Li, Y. Wang, Y. Zhang *et al.*, "Ultrathin MgB_2 films fabricated on Al_2O_3 substrate by hybrid physical-chemical vapor deposition with high T_c and J_c," Supercond. Sci. Technol. **24**(1), 015013 (2011).
[39]P. Focardi, A. Neto, and W. R. McGrath, "Coplanar-waveguide-based terahertz hot-electron-bolometer mixers improved embedding circuit description," IEEE Trans. Microw. Theory Tech. **50**(10), 2374–2383 (2002).
[40]P. Khosropanah, J. R. Gao, W. M. Laauwen, and M. Hajenius, "Low noise NbN hot electron bolometer mixer at 4.3THz," Appl. Phys. Lett. **91**, 221111 (2007).
[41]D. J. Hayton, J. R. Gao, J. W. Kooi, Y. Ren, W. Zhang, and G. de Lange, "Stabilized hot electron bolometer heterodyne receiver at 2.5 THz," Appl. Phys. Lett. **100**, 081102 (2012).
[42]We use an elliptical Si lens with the semi-minor axis of the ellipse *a* of 5 mm, the semi-major axis *b* of 5.235 mm, and the extension *c* from geometric center of the lens of 1.2 mm thick Si and 0.32 mm thick SiC substrate. This combination forms a nearly perfect elliptical lens based on the simulation by COMSOL Multiphysics. The refractive index is 3.38 for Si and 3.14 for SiC.
[43]Y. Gan, B. Mirzaei, S. van der Poel, J. R. G. Silva, M. Finkel, M. Eggens *et al.*, "3.9 THz spatial filter based on a back-to-back Si-lens system," Opt. Express **28**, 32693–32708 (2020).
[44]A. J. Gatesman, J. Waldman, M. Ji, C. Musante, and S. Yagvesson, "An anti-reflection coating for silicon optics at terahertz frequencies," IEEE Microw. Wirel. Compon. Lett. **10**(7), 264–266 (2000).
[45]H. Ekstrom, B. S. Karasik, E. L. Kollberg, and K. S. Yngvesson, "Conversion gain and noise of niobium superconducting hot-electron-mixers," IEEE Trans. Microwave Theory Tech. **43**(4), 938–947 (1995).
[46]The change of the HEB current is achieved by using the voice coil attenuator to vary the LO power at the HEB [41]. The advantage of this method is that the T_{rec}^{DSB} is not influenced by the fluctuations of the LO power and also the direct detection effect [56]. The latter is found to play no role in the MgB_2 HEBs because we have not seen any shifts in pumped IV curves between the hot and cold load. This is also what we expected since the radiation power between the two loads, to be absorbed by the HEB, is of the order of ∼10 nW, which is three orders of magnitude lower than the LO power (∼13 μW).
[47]E. Novoselov and S. Cherednichenko, "Gain and noise in THz MgB_2 Hot-electron bolometer mixers with a 30-K critical temperature," IEEE Trans. Terahertz Sci. Technol. **7**(6), 704–710 (2017).
[48]S. Cherednichenko, M. Kroug, H. Merkel, P. Khosropanah, A. Adam, E. Kollberg, D. Loudkov, G. Gol'tsman, B. Voronov, H. Richter, and H.-W. Huebers, "1.6 THz heterodyne receiver for the far infrared space telescope," Physica C **372–376**, 427–431 (2002).
[49]E. Novoselov, "Mgb_2 hot-electron bolometer mixers for sub-mm wave astronomy," Ph.D. thesis (Chalmers University of Technology, Sweden, 2014).
[50]D. E. Prober, "Superconducting terahertz mixer using a transition-edge microbolometer," Appl. Phys. Lett. **62**, 2119–2121 (1993).
[51]B. Mirzaei, W. J. Vreeling, J. R. G. Silva, W. Laauwen, and J. R. Gao, "Enhanced sensitivity of THz NbN hot electron bolometer mixers," in an Extensive Abstract, Submitted to 32nd IEEE International Symposium on Space THz Technology (ISSTT 2022), Baeza, Spain, *16–20 October* (IEEE, 2022).
[52]C. Zhang, D. Wang, Z.-H. Liu, Y. Zhang, P. Ma, Q.-R. Feng, Y. Wang, and Z.-Z. Gan, "Fabrication of superconducting nanowires from ultrathin MgB_2 films via focused ion beam milling," AIP Adv. **5**, 027139 (2015).
[53]H. L. Hortensius, E. F. C. Driessen, and T. M. Klapwijk, "Possible indications of electronic inhomogeneities in superconducting nanowire detectors," IEEE Trans. Appl. Supercond. **23**, 2200705 (2013).
[54]D. Wilms Floet, E. Miedema, T. M. Klapwijk, and J. R. Gao, "Hotspot mixing: A framework for heterodyne mixing in superconducting hot-electron bolometers," Appl. Phys. Lett. **74**, 433–435 (1999).
[55]H. F. Merkel, P. Khosropanah, D. Wilms Floet, P. A. Yagoubov, and E. L. Kollberg, IEEE Trans. Microwave Theory Tech. **48**, 690–699 (2000).
[56]J. J. A. Baselmans, A. Baryshev, S. F. Reker, M. Hajenius, J. R. Gao, T. M. Klapwijk, Y. Vachtomin, S. Maslennikov, S. Antipov, B. Voronov, and G. Gol'tsman, "Direct detection effect in small volume hot electron bolometer mixers," Appl. Phys. Lett. **86**, 163503 (2005).
[57]R. Schieder and C. Kramer, "Optimization of heterodyne observations using allan variance measurements," Astron. Astrophys. **373**, 746–756 (2001).
[58]M. Putti, M. Affronte, C. Ferdeghini, P. Manfrinetti, C. Tarantini, and E. Lehmann, "Observation of the crossover from two-gap to single-gap superconductivity through specific heat measurements in neutron-irradiated MgB_2," Phys. Rev. Lett. **96**, 077003 (2006).
[59]S. Cherednichenko, N. Acharya, E. Novoselov, and V. Drakinskiy, "Low kinetic inductance superconducting MgB_2 nanowires with a 130 ps relaxation time for single-photon detection applications," Supercond. Sci. Technol. **34**, 044001 (2021).
[60]Y. Lobanov, E. Tong, R. Blundell, A. Hedden, B. Voronov, and G. Gol'tsman, "Large-signal frequency response of an HEB mixer: From 300 MHz to terahertz," IEEE Trans. Appl. Supercond. **21**(3), 628–631 (2011).
[61]W. Miao, W. Zhang, J. Q. Zhong, S. C. Shi, Y. Delorme, R. Lefevre, A. Feret, and T. Vacelet, "Non-uniform absorption of terahertz radiation on superconducting hot electron bolometer microbridges," Appl. Phys. Lett. **104**, 052605 (2014).
[62]G. Ghigo, G. A. Ummarino, R. Gerbaldo, L. Gozzelino, F. Laviano, and E. Mezzetti, "Effects of disorder on the microwave properties of MgB2 polycrystalline films," Phys. Rev. B **74**, 184518 (2006).
[63]E. L. Kollberg, K. S. Yngvesson, Y. Ren, W. Zhang, P. Khosropanah, and J. R. Gao, "Impedance of hot-electron bolometer mixers at terahertz frequencies," IEEE Trans. Terahertz Sci. Technol. **1**, 383–389 (2011).
[64]D. C. Mattis and J. Bardeen, "Theory of the anomalous skin effect in normal and superconducting metals," Phys. Rev. **111**, 412–417 (1958).
[65]M. Shcherbatenko, I. Tretyakov, Y. Lobanov, S. N. Maslennikov, N. Kaurova, M. Finkel, B. Voronov, G. Goltsman, and T. M. Klapwijk, "Nonequilibrium

interpretation of DC properties of NbN superconducting hot electron bolometers," Appl. Phys. Lett. **109**(13), 132602 (2016).
[66]D. Wilms Floet, J. Baselmans, T. M. Klapwijk, and J. R. Gao, "Resistive transition of niobium diffusion-cooled Hot electron bolometers," Appl. Phys. Lett. **73**, 2826 (1998).
[67]P. G. de Gennes, "Boundary effects in superconductors," Rev. Mod. Phys. **36**, 225–237 (1964).
[68]C. Buzea and T. Yamashita, "Review of the superconducting properties of MgB_2," Supercond. Sci. Technol. **14**, R115–R146 (2001), where you are referred to Table 5 in page 19. We took only the coherence lengths ξ_c along c-axis for thin MgB_2 films, which is believed to be directly relevant to our system. Actually the coherence lengths along the ab plane (ξ_{ab}) range even larger.
[69]D. Wilms Floet, "Hotspot mixing in THz niobium superconducting hot electron bolometer mixers," Ph.D. thesis (Delft University of Technology, The Netherlands, 2001).
[70]S. L. Bud'ko, G. Lapertot, C. Petrovic, C. E. Cunningham, N. Anderson, and P. C. Canfield, "Boron isotope effect in superconducting MgB_2," Phys. Rev. Lett. **86**, 1877–1880 (2001).